NASA TN D-430



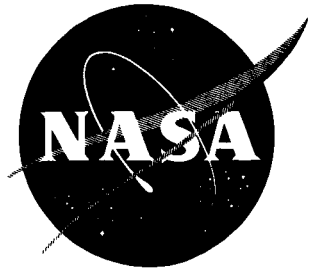


# TECHNICAL NOTE
## D-430

VIBRATION AND NEAR-FIELD SOUND OF THIN-WALLED CYLINDERS CAUSED BY INTERNAL TURBULENT FLOW

By Paul F. R. Weyers

California Institute of Technology

NATIONAL AERONAUTICS AND SPACE ADMINISTRATION

WASHINGTON

June 1960

NATIONAL AERONAUTICS AND SPACE ADMINISTRATION

TECHNICAL NOTE D-430

# VIBRATION AND NEAR-FIELD SOUND OF THIN-WALLED CYLINDERS CAUSED BY INTERNAL TURBULENT FLOW

By Paul F. R. Weyers

## SUMMARY

The present investigation concerned noise produced by turbulent flow adjacent to a flexible wall. Measurements of the spectrum and intensity of the pressure field outside thin-walled Mylar cylinders containing turbulent pipe flow have been made. The resulting spectra could be interpreted in relation to the elastic properties of the cylinders and the character of the turbulent fluctuations inside the flow. The eigen frequencies of the cylinders could be identified and similarity parameters for the spectra were established. The effect of cylinder wall thickness on the spectrum and intensity of the pressure fluctuations was investigated. It was found that the intensity of the external pressure field scaled with the fifth power of the velocity at the center of the pipe.

For one particular case the spectrum and intensity of the pressure fluctuations exerted by the turbulent flow on the wall were measured. The intensity of the pressure fluctuations at the wall scaled with the fourth power of the velocity as expected. The ratio of the root-mean-square wall pressure to the dynamic pressure was found to be independent of Mach number and equal to a constant (0.0078). Similarity laws for the spectra of the wall-pressure fluctuations were also confirmed.

## INTRODUCTION

The sound field inside aircraft in flight can be traced to a variety of sources, one of which is the turbulent airflow over the fuselage skin. It is a matter of practical experience that the boundary layer contributes little to the sound field inside the fuselage at speeds up to a few hundred miles per hour. Accordingly, in the past the problem of boundary-layer-induced cabin noise has not received much attention. However, the advent of high subsonic and supersonic commercial aircraft has stimulated interest in the mechanism of noise production by a turbulent boundary layer.

To develop the general idea underlying boundary-layer noise analysis, it is most convenient to start with the simplest case of air flowing past a rigid surface. In this case, the turbulent flow is the only source of sound. The sound is radiated into the free stream. This mechanism of sound generation has been discussed by Phillips (refs. 1 and 2) and by Curle (ref. 3) from a theoretical point of view; however, the analysis was handicapped by a lack of experimental information on the properties of the pressure fluctuations at a rigid wall. The first experimental data came from Willmarth (refs. 4 and 5), who measured the spectra and space-time correlation of the pressure fluctuations at a rigid wall for boundary layers of various thicknesses.[1] The experiments were made in a wind tunnel which was specifically designed for this purpose. The pressure fluctuations were measured with sophisticated barium titanate transducer equipment (ref. 7) over a Mach number range from 0.2 to 0.8. The measurements showed that the correlation function had a particular shape and that the pressure fluctuations at the wall were convected at an average speed of 0.82 times the free-stream speed. Also, Willmarth's results established that the correlation of the pressure fluctuations was destroyed in a downstream distance equal to approximately ten times the boundary-layer thickness.

In practice one usually deals with a flexible skin. It then becomes convenient to restrict the problem to the case of small skin deflections. In other words, the skin deflections are assumed small enough so that they will not induce time-dependent pressure gradients of the same order of magnitude as the forcing function (e.g., as in the case of panel flutter). Under these conditions, the forcing function on the flexible skin is essentially the same as if the skin were rigid.

The fluctuating forces on the wall, caused by the turbulent boundary layer, are the wall static pressure and the shearing stress. However, it is usually assumed that for thin skins the wall transmits pressure only by deflecting laterally. Consequently, the effects of shear stress may be ignored in this case.

The process of transmission of boundary-layer noise through the thin flexible skin can then be thought of as follows: The random fluctuating wall pressure acts as a driving force on the skin, pushing the elastic skin in and out. In turn, the motion of the skin acts as a set of distributed pistons, creating a pressure field in the stationary medium which constitutes the "cabin."

In order to simplify the analysis one usually assumes that the motion of the skin is described by a linear equation. Also, it is assumed that generation of a random pressure field in the stationary

---

[1]Einstein and Li, reference 6, previously measured the autocorrelation of wall-pressure fluctuations of oil flow in an open channel flume.

medium is a linear radiation problem. The mathematical techniques for solving the problem are similar to those required to calculate the response of a linear system to a stochastic forcing function of several variables.

The above approach was taken by Corcos and Liepmann (ref. 8). They considered the radiation of sound from a large randomly vibrating flat plate excited by a turbulent boundary layer. The problem has also been considered by Kraichnan (refs. 9, 10, and 11) and Ribner (ref. 12). Both authors assumed a given spectral distribution for the pressure fluctuations in the boundary layer. Also, both assumed that the pressure fluctuations were convected. Kraichnan treated the skin as an assembly of flat square sections which vibrate independently, while Ribner considered an infinite sheet. Kraichnan and Ribner worked with a spectral function; Corcos and Liepmann preferred to work with the correlation function.



Unfortunately, the theoretical treatment of all models required many assumptions because of an almost complete lack of any experimental data on the transmission of pressure fluctuations across a flexible skin. Also, at the time the above reports were written no data on the properties of the wall pressure were available.

It became desirable to obtain experimental information on this matter. A first step in such a program is the selection of a suitable skin configuration, and various configurations were considered. It was decided to work with a thin-walled cylinder rather than with a thin flat plate. One obvious advantage of a vibrating cylinder is the axial symmetry of its external pressure field. Furthermore, it was decided to make the flow inside the cylinder fully developed turbulent pipe flow. Pipe flow was chosen because of the existence of excellent experimental data on the structure of turbulence in pipes (ref. 13).

The general aim of the present experimental investigation was to make an exploratory study of the transmission of pressure fluctuations through an elastic skin.

The power spectrum of the pressure fluctuations in the stationary medium outside the vibrating cylinder is a function of the power spectrum of the wall pressure and the impedance of the thin-walled cylinder. The power spectrum of the pressure at the wall of a cylinder containing fully developed pipe flow has never been measured. Also, little is known about the impedance of thin-walled cylinders of finite length. One could argue intuitively that, for a certain forcing function, the impedance of a finite cylinder depends on its length, diameter, thickness, boundary conditions, material properties, and damping. It would take many experiments to investigate the effect of each of these variables.

The present work was restricted to an investigation of the following points:

(1) The spectrum and intensity of the pressure fluctuations at the wall of an elastic cylinder.

(2) The effect of wall thickness on the spectrum and intensity of the pressure fluctuations at a point outside an elastic cylinder.

(3) The effect of wall thickness and pressure difference across the wall on the natural frequencies of vibration of a cylinder. The length, diameter, boundary conditions, and material of the cylinder were not changed in the experimental program.



The present investigation was conducted at the Guggenheim Aeronautical Laboratory of the California Institute of Technology under the sponsorship and with the financial assistance of the National Advisory Committee for Aeronautics as part of a long-range aerodynamic noise study directed by Dr. H. W. Liepmann. The advice, criticisms, encouragement, and assistance of the Drs. H. W. Liepmann, W. W. Willmarth, and Y. C. Fung, and Mr. G. T. Skinner, and Mrs. Dorothy Diamond are gratefully acknowledged. In addition, discussions with Dr. G. M. Corcos of the University of California were much appreciated and proved to be very useful in interpreting some of the results.

## SYMBOLS

| | |
|---|---|
| $c$ | variable |
| $d$ | diameter of cylinder, 1 in. |
| $E$ | Young's modulus of Mylar, 550,000 psi |
| $f$ | natural frequency of vibration of cylinder, cps |
| $f(x_p,z_p,t)$ | random force per unit mass exerted by pressure fluctuations on flat plate |
| $F(k_1,k_2,\omega)$ | spectrum density of wall pressure in space and time |
| $F(n)$ | spectrum density of pressure fluctuations in time |
| $k_1,k_2$ | wave numbers in $x_p$ and $y_p$ directions, respectively |
| $K_1,K_2$ | wave numbers in $x$ and $\varphi$ directions, respectively |

| | |
|---|---|
| $l$ | number of circumferential waves in cylinder |
| L | length of Mylar cylinder, 11 in. |
| m | number of axial half waves in cylinder |
| n | frequency, cps |
| $\bar{n}_x$ | nondimensional axial tension in shell due to internal pressure, $\frac{\bar{N}_x}{E\tilde{t}}$ |
| $\bar{n}_\varphi$ | nondimensional circumferential tension in shell due to internal pressure, $\frac{\bar{N}_\varphi}{E\tilde{t}}$ |
| $\bar{N}_x$, $\bar{N}_\varphi$ | stress resultants in shell due to internal pressure, force per unit length |
| $p_d$ | static pressure difference across cylinder wall |
| p | instantaneous value of pressure fluctuations |
| q | dynamic pressure, $\frac{1}{2}\rho U_o^2$ |
| Re | Reynolds number |
| r | radial distance from center of cylinder |
| t | time |
| $\tilde{t}$ | thickness of cylinder wall |
| U | mean velocity at any point in pipe |
| $U_o$ | maximum value of mean velocity |
| u' | velocity fluctuation in axial direction |
| $V_n$ | normal velocity of skin element |
| v' | velocity fluctuation in radial direction |
| w' | velocity fluctuation in tangential direction |

| | |
|---|---|
| $\overline{\left(\frac{\partial V_n}{\partial t}\right)^2}$ | mean square acceleration of skin element |
| $X_p(k_1,k_2,\omega)$ | impedance of flat plate |
| $X(K_1,K_2,\omega)$ | impedance of cylinder |
| $x_p$ | coordinate along flat plate in free-stream direction |
| $x$ | longitudinal coordinate along pipe |
| $y_p$ | skin deflection normal to flat plate |
| $y$ | skin deflection of cylinder wall in radial direction |
| $z_p$ | coordinate along flat plate normal to free-stream direction |
| $\Gamma$ | admittance of cylinder wall |
| $\eta$ | attenuation coefficient |
| $\lambda_c$ | nondimensional parameter, $\frac{m\pi d}{2L}$ |
| $\nu$ | kinematic viscosity of air |
| $\rho$ | density of air |
| $\rho_s$ | density of Mylar, 0.05 lb/in.$^3$ |
| $\sigma$ | Poisson's ratio of Mylar, 0.316 |
| $\tau$ | time internal |
| $\varphi$ | azimuthal coordinate |
| $\phi_1(nd/U_o)$ | nondimensional spectral function |
| $\phi_2(n/n_o)$ | nondimensional function |
| $\phi_3(n/n_o)$ | nondimensional function |
| $\psi(\tau)$ | autocorrelation function |
| $\omega$ | frequency, radians/sec |

# APPARATUS AND METHODS

## Pipe Facility

The present investigation was carried out using the apparatus shown in figure 1. The available air supply was filtered by a Norgren air pressure regulator, which is a high-capacity regulator of the balanced-diaphragm type. The output of the regulator was controlled by means of a separate high-precision pilot regulator which was operated manually. After leaving the regulator, the air was passed through a muffler. The purpose of the muffler was to absorb the noise produced in the supply system by the valves of the pressure regulator. The sound absorption process was done at approximately one-tenth of the air speed in the pipe proper. The contraction at the end of the muffler accelerated the low-noise air into a 1-inch-diameter seamless brass pipe 8 feet long with a wall thickness of 1/4 inch. Fully developed turbulent flow was established in the pipe. Between sections of the pipe, a short, very thin-walled section was inserted through which pressure disturbances could pass readily into an enclosure containing a microphone. The enclosure was lined with Fiberglas and acted as a small-scale anechoic chamber. The air was then exhausted through another muffler placed around the exit of the pipe. The purpose of the second muffler was to absorb any jet noise.

## Muffler System

The muffler originally consisted of a 10-inch-diameter steel casing 7 feet long. The 10-inch-diameter section was reduced in two stages to a 1-inch-diameter section by means of concentric swage nipples. The acoustic lining inside the casing consisted of a $3\frac{7}{8}$-inch-thick Fiberglas blanket of 3 $lb/ft^3$ density, bonded together by thermosetting plastic resin. The Fiberglas was held in place by a rolled sheet of punched aluminum, 0.023 inch thick, with 3/32-inch-diameter holes on 1/4-inch centers. The inner aluminum lining did not appreciably reduce the effectiveness of the Fiberglas blanket. The air passed through the 3-inch-diameter aluminum tube.

The sound-absorption characteristics of the muffler were checked as follows. A loudspeaker, driven by an oscillator and amplifier, was connected to one end of the muffler, the other end being sound-insulated. For a constant loudspeaker input, the sound level inside the muffler was measured with an Altec-Lansing 21-BR-150 condenser microphone at various points in the muffler. The results of the test are shown in figure 2.

As expected, the muffler was not very efficient in absorbing sound under 200 cps; however, as far as the experiment was concerned, the

frequency range from 0 to 200 cps is of little interest. It can also be seen from figure 2 that at the higher frequencies, say above 6,000 cps, the muffler is not quite so efficient as in the range from 200 to 6,000 cps. This may be due to resonances in the cross section of the 3-inch-diameter aluminum tube. In order to make sure that the higher frequencies were sufficiently absorbed, the muffler was modified. Two baffles were added, as shown in figure 1, and the muffler was lengthened as well. It is a well-known fact that baffles or bends in an acoustic system are very good high-frequency sound absorbers. It was calculated that the bends provided an additional attenuation of at least 40 decibels.



## Thin-Walled Cylinder

The thin-walled section which transmits the pressure disturbances was originally made of paper; however, the use of paper was found to be unsatisfactory because it absorbed the moisture in the air. A new material known as Mylar was then used. It is a polyester film made by the E. I. du Pont de Nemours & Co., Inc. The advantages of Mylar are:

(1) The density is low, about one-half that of aluminum.

(2) It is available in small thicknesses, ranging from 0.00025 to 0.0075 inch.

(3) It does not absorb moisture.

(4) It has a low Young's modulus, namely, 550,000 psi.

(5) It has a high tensile strength, approximately 20,000 psi.

(6) Its physical properties are uniform in almost every sheet of material.

In the present work four different thicknesses were used, that is, 0.0005, 0.001, 0.0015, and 0.0021 inch.

The Mylar cylinders were made and installed as follows. A sheet of Mylar was rolled onto a 1-inch-diameter steel rod, and the edges were cemented together in a lap joint. The width of the joint was approximately 1/4 inch. Two bushings were cemented to the Mylar tube and the former were locked to the steel rod as shown in figure 3. The whole unit was then slid into the anechoic chamber.

## Anechoic Chamber

The bushings were held in place by means of lock screws as shown in figure 4. Finally, the steel rod was withdrawn leaving the Mylar cylinder perfectly located inside the chamber. The two 1-inch-diameter pipe sections were then coupled to the anechoic chamber. This technique satisfied both the acoustic and aerodynamic requirements of a smooth continuous joint between the brass pipe and the Mylar tube.

To make sure that the Mylar tube was not appreciably affected by any mechanical vibrations O-rings were used throughout the system.

It was decided to use an anechoic chamber rather than a reverberation chamber because with a reverberation chamber it would have been difficult to distinguish between the natural frequencies of the chamber and those of the vibrating cylinder. The present Fiberglas configuration inside the chamber was chosen to insure that the microphone measured the pressure field set up by the vibrating wall element directly underneath it. The sound field was essentially at normal incidence to the microphone, the sound field in the other directions being absorbed by the Fiberglas lining.

If the acoustic lining had been merely a thin strip along the wall of the chamber, then the microphone would have discriminated against the high-frequency sound coming from the ends of the vibrating tube because the radiation pattern of high-frequency sound from a source is very directional. There was one more reason for the choice of this particular Fiberglas configuration. It is well known that the response of the microphone is more or less the same for low-frequency waves irrespective of their angle of incidence. This is not so at high frequencies. Of course, the above considerations would not have been important if a short cylinder had been used in the experiment; however, a short cylinder would have put a severe constraint on the possible modal configuration. That is, a short tube would have discriminated against radiation of sound at the longer wave lengths.

## Measurement of Mean Velocity and Pressure

The mean velocity profile at a station a few diameters downstream of the test section was measured with a small total-head tube. The probe was made of 0.04-inch-diameter nickel tube stock with 0.003-inch wall thickness. The tip of the probe was flattened to an opening of 0.007 inch. In the measurements the static pressure was assumed constant across the pipe. It was measured at the wall and in the same cross-sectional plane as the mouth of the total-head tube. A typical velocity profile is shown in figure 5.

It was noted that the presence of the total-head tube in the pipe produced sharp peaks in the spectrum of the pressure fluctuations outside the Mylar tube. Subsequently, the probe was removed and the static pressure at the wall at a station 100 diameters upstream of the test section was calibrated against the mean velocity at the center of the pipe at the microphone station.

The static-pressure distribution in the direction of the flow was measured through pressure taps located on both sides of the test section. It was found that approximately 30 minutes were needed to measure each power spectrum of the external pressure field, and 30 minutes were considered a minimum in order to provide adequate time averaging. It thus became necessary to check whether the pressure regulator system was capable of maintaining constant velocity in view of the fluctuating campus supply pressure. It was found experimentally that the pressure regulator was able to hold the mean velocity at the center of the pipe to within ±1/2 percent in a range from 100 to 450 feet per second. In the experiments the mean velocities varied from approximately 120 to 350 feet per second.



## Microphone Equipment

An Altec-Lansing 21-BR-150 condenser microphone was used for all pressure measurements at points outside the cylinder. The diameter of the microphone button was approximately 5/8 inch. The microphone was separated from the anechoic chamber by means of a thick rubber lining to avoid vibration pickup. The microphone was calibrated up to 40,000 cps for normal incidence sound waves by the Western Electro-Acoustic Laboratory in Los Angeles (fig. 6). The weakness of the sound field outside the vibrating cylinder necessitated the use of a condenser microphone system. However, the measurement of the pressure fluctuations at the wall of a Mylar cylinder was made with a barium titanate transducer.

The barium titanate transducer used in the present work was designed by Willmarth (ref. 7). It consisted of two barium titanate disks cemented into a recess in a brass fitting. The gap around the disks was sealed by a thin coating of radio cement covering the exposed surface. The diameter of the barium titanate element was approximately 5/32 inch and the thickness of each disk was 0.040 inch. The outside diameter of the brass fitting was approximately 5/16 inch. The outer face of the element was slightly concave to allow for the curvature of the pipe. The barium titanate pressure transducer assembly is shown in figure 7.

The transducer was calibrated in a shock tube and the sensitivity was found to be $0.76 \times 10^{-6}$ volts/dyne/cm$^2$. Its frequency response was flat from approximately 5 to 50,000 cps. A detailed description of the transducer, that is, its design and method of calibration may be found in reference 7.

## Electronic Equipment

It became necessary to develop a low-noise cathode-follower preamplifier for use with the barium titanate transducer. The noise level of the preamplifier was $5 \times 10^{-6}$ volts for the band from 0 to $\infty$ cps. The frequency response of the preamplifier was found to be flat within ±2 percent over the range 300 to 50,000 cps. The gain of the preamplifier over this range was 47. The preamplifier circuit is shown in figure 8. In addition, a second amplifier was used which had a flat frequency response from 10 to $10^5$ cps. Since the band width of the latter amplifier was considerably wider than that of the preamplifier, the response of the combination was flat within ±2 percent over the range from 300 to 50,000 cps.



The wave analyzer used in the experiment was a Donner Model 21 wave analyzer having a constant band width from 30 to 50,000 cps. The band-pass characteristics of this instrument are shown in figure 9.

The measurements taken with the Altec-Lansing 21-BR-150 condenser microphone did not require use of the preamplifier because in this case there was no signal-to-noise ratio problem. Also, the Altec microphone contained its own cathode follower and hence no additional cathode follower was necessary. However, the amplifier mentioned above was used to boost the output voltage of the Altec microphone. The only other electronic equipment employed in the present work were a variable band-pass filter (Krohn-Hite Model 310-AB), a vacuum-tube voltmeter (Hewlett-Packard Model 400 C), and an oscilloscope.

# GENERAL CONSIDERATIONS

## Response of a Linear System to a Random Force

The response of the elastic skin of the Mylar cylinder to the internal wall-pressure fluctuations can be studied qualitatively by considering a simple problem.

It is instructive to study the response of a linear system to a random forcing function of several variables (refs. 8, and 14 to 18). As an example, consider the response of a large flat plate excited by a turbulent boundary layer. This particular problem was analyzed by Corcos and Liepmann (ref. 8).

Suppose that the motion of the plate is described by a linear differential equation in $y_p$. Let $f(x_p, z_p, t)$ be the random force per unit mass exerted by the pressure fluctuations in the boundary layer on the

plate. The forcing function $f(x_p,z_p,t)$ is characterized by its power spectral density $F(k_1,k_2,\omega)$ which is assumed to be a continuous function of the wave numbers $k_1$ and $k_2$ (in the $x_p$ and $z_p$ direction) and of the frequency $\omega$, that is

$$\overline{f(x_p,z_p,t)^2} = \int_0^\infty \int_{-\infty}^\infty \int_{-\infty}^\infty F(k_1,k_2,\omega)\, dk_1\, dk_2\, d\omega \qquad (1)$$

In the present work the configuration under consideration was a thin-walled cylinder and not a flat plate. The arguments pertaining to the case of a flat plate hold qualitatively for the case of a thin-walled cylinder containing turbulent flow; however, the analogy with the flat plate is less direct because of circumferential restrictions on the cylinder.

If the length of the cylinder is finite, it is no longer permissible to ignore the end conditions. Physically it means that axial standing waves occur in addition to circumferential standing waves. The cylinder exhibits resonance at a set of discrete frequencies corresponding to the natural frequencies of vibration.

In the lowest frequency range the natural frequencies are quite discrete. As the number of axial and circumferential modes increases, the difference between consecutive natural frequencies decreases rapidly. Eventually the natural frequencies are bunched so closely that they approach the limit of continuous resonance. When this happens, the spectrum of the mean-square wall deflection is smooth and conditions approach those of the idealized model discussed above, hence the spectrum of the pressure fluctuations at a point outside the cylinder is expected to show several peaks at the lower frequencies followed by an increasingly smooth spectrum at the higher frequencies.

The investigation was primarily concerned with the measurement and analysis of the pressure fluctuations at the higher frequencies.

The response of the cylinders at the lower frequencies, that is, the occurrence and nature of the discrete frequencies of vibration, is analyzed in the appendix.

Now suppose that the plate is large enough compared with the correlation length of the wall-pressure fluctuations that the average plate motion is not sensibly affected by the end conditions. Under these conditions one may use a result from generalized Fourier analysis which states that for a function defined by its power spectrum and mean values, one may write:

$$\overline{y_p^2} = \int_0^\infty \int_{-\infty}^{\infty} \int_{-\infty}^{\infty} \frac{F(k_1,k_2,\omega)\,dk_1\,dk_2\,d\omega}{\left|X_p(k_1,k_2,\omega)\right|^2} \qquad (2)$$

The above equation describes the relation between the power spectrum of the input $F(k_1,k_2,\omega)$, the mean-square deflection $\overline{y_p^2}$ (or output), and the square of the absolute value of $X_p(k_1,k_2,\omega)$.

The value of $1/\left|X_p(k_1,k_2,\omega)\right|^2$ can be calculated. It is the square of the Fourier transform of the fundamental solution of the linear differential equation for the skin deflection. Hence, in order to obtain the response of a linear system to a random forcing function one has to know the impedance of the system and the power spectrum of the forcing function.

It is obvious that resonance will occur whenever the term $\left|X_p(k_1,k_2,\omega)\right|^2$ assumes a minimum value. In fact, it can be shown (ref. 8) that, for an infinite plate, resonance occurs continuously over the whole frequency spectrum. In other words, if the spectrum of the input is "smooth," then in the idealized case the spectrum of the output cannot show any sharp peaks.

## EXPERIMENTAL RESULTS

### Pressure Fluctuations at Cylinder Wall

The measurement of the pressure fluctuations at the wall of the cylinder was made as follows. As shown in figure 7, the slightly concave face of the transducer was pressed against the skin of a Mylar cylinder having a wall thickness of 0.0005 inch. In other words, the skin was in direct contact with the barium titanate element at all times. The method is unorthodox and needs clarification.

The contact of the transducer with the skin obviously affected the motion of the skin by creating a nodal point at the place of contact. However, in this particular measurement one is not interested in the motion of the skin nor in the external pressure field. The quantity of interest was the spectrum of the internal pressure fluctuations at the wall of the cylinder. Assuming small skin deflections, the properties of the pressure fluctuations at the wall were not sensibly affected by the motion of the skin. The presence of the skin on top of the barium titanate element obviously gave rise to a certain degree of attenuation. However, the wall thickness was very thin, namely 0.0005 inch, and the density of the

material was low. Also, the stiffness of a Mylar sheet is very small compared with the stiffness of the barium titanate element. Accordingly, the above method, although not ideal, may be expected to yield reasonably accurate information on the properties of the wall pressure in turbulent pipe flow. This view is supported by the experimental results. Two typical power spectra of the pressure fluctuations at the wall are plotted in figure 10.

## Pressure Field at Point Outside Cylinder

Originally, it had been intended to measure the sound level in both the "near field" and the "far field." However, it became evident that the sound level in the far field was much too weak for measurement with any type of pressure pickup. In fact, even at a few diameters away from the center of the pipe, the pressure field, although measureable, was still weak. It was decided to make all pressure measurements outside the cylinder at a station 3/4 inch from the center of the pipe, where the distance from the wall to the microphone was 1/4 inch.

The pipe exhausts to atmosphere and the pressure in the anechoic chamber is also atmospheric. Hence as the velocity is increased, the pressure difference across the thin-walled cylinder is increased. Consequently the diameter of the elastic cylinder increased a little with increased internal pressure. The increase in diameter for the thinnest cylinder, 0.0005-inch wall thickness, was measured to be 0.01 inch. It was felt that this small decrease in distance between the microphone and the cylinder wall did not appreciably affect the magnitude of the observed pressure fluctuations at the microphone station.

Two sets of power spectra of the external pressure for cylinders of wall thickness 0.0005 inch and 0.001 inch are shown in figure 11.

The logarithm of the root-mean-square pressure at the wall is plotted against the logarithm of the velocity at the center of the pipe in figure 12, and the logarithm of the root-mean-square pressure at the station $r/d = 3/4$ is plotted against the logarithm of the velocity at the center of the pipe in figure 13. The experimental results show that the mean-square pressure is proportional approximately to the fifth power of the velocity.

Next, a curve of best fit was drawn through the smooth high-frequency part of each power spectrum. It was found that, for each cylinder, the curves scaled if the parameter $\frac{F(n)}{\rho^2 U_o^4}$ was plotted as a function of $\left(\frac{nd}{U_o}\right)$. As stated before, the diameter of the cylinder was not varied with experiments. The velocity in most tests was changed by a ratio of approximately 2 to 1.

The results of this phase of the work are shown in figure 14 for cylinders of wall thickness 0.0005, 0.001, 0.0015, and 0.0021 inch, respectively.

## DISCUSSION

### Pressure Fluctuations at Wall

The existence of fully developed turbulent flow in a pipe implies that the velocity profile has approached a universal form. The dominant variables that describe the mean turbulent flow are $\rho$, $U_o$, and $d$.

The pipe flow experiments of Laufer (ref. 13) established that the turbulent velocity fluctuations $u'$, $v'$, $w'$ are proportional to $U_o$ and that the correlation function does not depend on $U_o$.

The pressure fluctuation $p'$ is proportional to $\rho u'u'$ and hence one pressure can be formed proportional to $\rho U_o^2$ and one length, proportional to $d$.

In the present work the magnitude of the mean velocity was sufficiently low to warrant the assumption of incompressible flow. Accordingly one would expect the mean-square wall pressure to be proportional to $U_o^4$. This was checked experimentally, and the result is shown in figure 12. It was found that the ratio of the root-mean-square pressure to the dynamic pressure was a constant (0.0078). (Willmarth (ref. 5) found that the ratio of root-mean-square wall pressure to dynamic pressure was a constant (0.006) for a turbulent boundary layer.)

An examination of the power spectra (fig. 10) indicates the existence of one or two sharp peaks in each spectrum. It is felt that the peaks are not associated with the internal flow. Also, since the transducer response is flat between 5 to 50,000 cps they cannot be traced to the transducer either. The transducer touched the cylinder and it is thought that the finite size of the transducer put a constraint on the motion of the skin causing a disturbance which was fed to the barium titanate element in the form of a sharp peak.

### Similarity Parameters

The selection of nondimensional parameters for the case of pressure fluctuations at the wall was arrived at as follows.

The mean-square pressure at the wall can be written in its power spectral form

$$\overline{p^2} = \int_0^\infty F_1(n)dn \tag{3}$$

If the skin deflection is small the wall pressure is a function of the internal flow variables only and not of the elastic properties and constraints of the cylinder. From the preceding discussion it is seen that the mean-square wall pressure is proportional to $\rho^2 U_o^4$ and that the problem has one characteristic length proportional to d.

In order to describe the spectral properties of the pressure fluctuations it is necessary to make a statement about the frequency. It is assumed that a characteristic frequency $n_o$ for the pressure fluctuations is proportional to $U_o/d$, that is, the characteristic frequency

$$n_o = \frac{U_o}{d} \tag{4}$$

Hence equation (3) may be written as

$$\overline{p^2} = \int_0^\infty F_1(n)dn = \rho^2 U_o^4 \int_0^\infty \phi_1\left(\frac{n}{n_o}\right) d\left(\frac{n}{n_o}\right) \tag{5}$$

so that

$$\phi_1\left(\frac{nd}{U_o}\right) = \left(\frac{F_1(n)}{\rho^2 U_o^4}\right)\left(\frac{U_o}{d}\right) \tag{6}$$

The universal function $\phi_1\left(\frac{nd}{U_o}\right)$ is determined from the experiments. The smooth part of each power spectrum, say above 1,000 cps as shown in figure 10, was plotted in nondimensional form in figure 15. The plot in figure 15 shows that the spectra scaled with velocity as prescribed by equation (6). The scaling of the spectra with diameter was not investigated.

The scaling laws for the pressure fluctuations outside the Mylar cylinder were derived in a similar fashion; however, now one has to include the effect of the cylinder wall.

For a given cylinder, that is, given elastic properties and constraints, the mean-square pressure at a given distance away from the pipe is written as

$$\overline{p^2} = \int_0^\infty F(n)dn \tag{7}$$

The spectral density function $F(n)$ can be expressed as a product of $\Gamma(n)$, a term proportional to the admittance of the cylinder, and $F_1(n)$, the spectral density of the pressure fluctuations at the wall,

$$F(n) = \Gamma(n)F_1(n) \tag{8}$$

For the case of the external pressure field, it is useful to deal with two characteristic frequencies. One frequency is the characteristic frequency of the flow $n_o = \frac{U_o}{d}$ which has already been discussed. The other is the characteristic frequency of the material $n_1$, where

$$n_1 = \frac{c}{d} \tag{9}$$

The variable $c$ is assumed to be a characteristic velocity which depends on the elastic properties of the material.

Hence equation (7) can be written as

$$\overline{p^2} = \int_0^\infty F(n)dn = \rho^2 U_o^4 \int_0^\infty \psi\left(\frac{n}{n_o}, \frac{n_o}{n_1}\right) d\left(\frac{n}{n_o}\right) \tag{10}$$

so that

$$F(n) = \frac{\rho^2 U_o^4}{n_o} \psi\left(\frac{n}{n_o}, \frac{n_o}{n_1}\right) \tag{11}$$

The form of $F_1(n)$ in equation (8) is given by equation (6). If one assumes that the function $\Gamma(n)$ in equation (8) is of form

$$\Gamma(n) = \frac{n_o}{n_1} \phi_2\left(\frac{n}{n_o}\right)$$

then one can write equation (11) as

$$F(n) = \frac{\rho^2 U_o^4}{n_o} \frac{n_o}{n_1} \phi_3\left(\frac{n}{n_o}\right) \tag{12}$$

The object of this simple analysis was to find scaling laws for the spectra of the pressure fluctuations if the flow velocity was varied in a cylinder of fixed size and material. Since the cylinder configuration was fixed, only one typical length was needed for dimensional purposes. The diameter of the pipe was chosen as the characteristic length because it is associated with the flow characteristics.

Equation (12) suggests that the spectra of the pressure fluctuations outside the cylinder scale with flow velocity if the spectral function $\frac{F(n)}{\rho^2 U_o^4}$ is plotted against the nondimensional parameter $\frac{nd}{U_o}$.

Substitution of equation (12) into equation (7) gives the relation

$$\overline{p^2} = \frac{\rho^2 U_o^5}{c} \int_0^\infty \phi_3\left(\frac{n}{n_o}\right) d\left(\frac{n}{n_o}\right) \tag{13}$$

Hence, for a given cylinder, the mean-square pressure at a given distance from the cylinder varies as the fifth power of the velocity.

## External Pressure Field

It is interesting to compare the power spectra of the internal pressure fluctuations at the wall with those measured outside the cylinder. The spectra of the pressure fluctuations measured outside the cylinder pass through the origin, show several sharp peaks, and extend over a wide frequency range. In contrast, the power spectra of the pressure measured at the wall do not pass through the origin and do not extend over as wide a frequency range. Also, most of their energy is contained at the lower frequencies. The reason for the power spectrum passing through the origin and extending over a wide frequency range in one case and not in the other may be explained qualitatively as follows.

Equation (2) suggests that the mean-square skin deflection $\overline{y^2}$ of the cylinder is of the following form:

$$\overline{y^2} = \iiint \frac{F(K_1, K_2, \omega)\, dK_1\, dK_2\, d\omega}{\left|X(K_1, K_2, \omega)\right|^2}$$

where $F(K_1,K_2,\omega)$ is the power spectrum of the wall pressure and $X(K_1,K_2,\omega)$ is the impedance of the cylinder. Now, the mean-square pressure $\overline{p^2}$ outside the cylinder is proportional to the mean-square normal acceleration of a typical vibrating cylinder wall element. Therefore, one may write

$$\overline{\left(\frac{\partial V_n}{\partial t}\right)^2} = \overline{\left(\frac{\partial^2 y}{\partial t^2}\right)^2} = \iiint \frac{\omega^4 F(K_1,K_2,\omega)\,dK_1\,dK_2\,d\omega}{\left|X(K_1,K_2,\omega)\right|^2} \qquad (14)$$

The effect of the $\omega^4$ term in the numerator is to force the power spectrum to pass through the origin, and in addition it raises the very high-frequency part of the spectrum.

The dependence of $\overline{p^2}$ on the velocity is shown in figure 13. The experimental results show that $\overline{p^2}$ is proportional to $U_o^5$, approximately. The author tested eight cylinders of different wall thickness ranging from 0.0005 to 0.0021 inch. In these tests the exponent of the velocity varied from a value of 4.8 to a value of 5.15. In six out of eight cases the range of the exponent varied from 4.9 to 5.10.

The repeatability of the total root-mean-square pressure measurements was surprisingly good considering that the cylinders could not be made exactly the same even though their wall thicknesses were identical. The results were repeatable within ±5 percent. A typical result is shown in figure 13(d).

A curve of best fit was drawn through the smooth high-frequency part of each power spectrum. Typical examples are shown in figure 11. It was found that this particular section of each power spectrum scaled with velocity if the power spectral function $F(n)/\rho^2 U_o^4$ was plotted against the nondimensional parameter $nd/U_o$ for each cylinder. The results are shown in figure 14.

The repeatability of power spectra measurements was reasonably good. For instance, all power spectra could be reproduced within ±7 percent. A typical case is shown in figure 14(e). The repeatability of the power spectra measurements was not as good as that of the measurements of $\overline{p^2}$ versus velocity because the latter measurements could be taken in a relatively short time whereas a period of approximately 30 minutes was needed for each spectrum. During this time the mean velocity in the pipe varied by 1 percent. Also, the use of the wave analyzer introduced additional errors.

In all tests, the lower limit of velocity was usually dictated by intensity requirements. The upper limit was set by "bursting" strength limitations of each thin-walled cylinder.

A curve of best fit was drawn through each of the sets of power spectra shown in figures 14(a), 14(b), 14(c), and 14(d).

An attempt was made to find a scaling parameter which would include the effect of wall thickness. One would expect that at the higher frequencies the transmission of the pressure fluctuations is primarily governed by the mass of the tube wall, $\overline{p^2} \propto \tilde{t}^{-2}$. Consequently, if the spectral function $F(n)\rho^{-2}U_o^{-4}$ is multiplied by $\tilde{t}^2$, one would expect reasonably good scaling. This plot is shown in figure 16(a).

However, it is not obvious that the phenomena are quite that simple. The response of an oscillating system is either stiffness-, resistance-(damping), or mass-controlled depending on whether the driving frequency is less than, equal to, or greater than the natural frequency (ref. 19). This is the reason that, at the higher frequencies, one would first try a scaling parameter based on the mass law.

However, in the present case, the smooth part of the spectrum at the higher frequencies may be interpreted as a "continuous" resonance (ref. 8). If this is correct, damping may play an important role. Hence it is not completely certain whether the mass law dominated the phenomena.

An analysis was made for the case of an infinite flat membrane where the effect of air damping was included. The damping constant was assumed to be inversely proportional to the wall thickness. The analysis was similar to the one carried out by Corcos and Liepmann (ref. 8) for the infinite flat plate. The calculations suggested a plot of $F(n)\rho^{-2}U_o^{-4}\tilde{t}$ versus $ndU_o^{-1}\tilde{t}^{1/2}$. The plot is shown in figure 16(b). The analysis involved many assumptions. Also the actual configuration is cylindrical rather than planar. In addition, it is not certain that the tubes behaved as membranes.

For instance, for the tube of wall thickness 0.0005 inch, table I shows that various and appreciable amounts of energy went into stretching of the shell and, therefore, the tension may no longer have been constant.

Although the model was not a good one, the fact remains that the spectra for the various wall thicknesses could be made to fall together by using two different sets of scaling parameters (fig. 16).

Hence the only conclusion one may draw is that, in the present experiment, the effect of wall thickness on the transmission of the pressure fluctuations is not well understood.

An inspection of the power spectra (fig. 11) shows the existence of a "hump" in the spectrum around 8,000 to 9,000 cps. Upon investigation it was found that the hump increased in amplitude with increased wall thickness. It did not shift in frequency with increased speed. Also, as the Fiberglas lined cavity in which the microphone was located was increased in size, the hump tended to disappear. Accordingly it was thought that the phenomena were associated with some kind of damped resonance inside the acoustic cavity. Consequently, the presence of the hump was ignored.



It is realized that the anechoic properties of the Fiberglas lined chamber are not perfect. However, it should be borne in mind that the pressure fluctuations occur at high frequencies and the absorption characteristics of Fiberglas at high frequencies are reasonably good. The radiated sound field is essentially very weak and it is felt that although some reverberation may have occurred at the lower frequencies the overall reverberation effects were small.

The weakness of the external sound field may be explained as follows. It is thought that the running ripples in the cylinder wall were heavily damped. Three forms of damping may have occurred. However, it is thought that the effects of both structural and aerodynamic damping were small compared with the damping which occurred because the correlation function of the forces was related over a distance.

The latter can cause considerable cancellation of forces acting on the cylinder wall, thus resulting in weak external sound fields.

## CONCLUSIONS

An investigation of the vibration and near-field sound of thin-walled cylinders caused by internal fully developed turbulent pipe flow was made. In the experiments the cylinder wall deflection was kept small compared with the diameter. The experimental results led to the following conclusions.

1. The spectra of the pressure fluctuations at the wall of the pipe can be represented by the relation

$$\phi_1\left(\frac{nd}{U_o}\right) = \left(\frac{F_1(n)}{\rho^2 U_o{}^4}\right)\left(\frac{U_o}{d}\right)$$

where $\phi_1(nd/U_o)$ is the universal function, $F_1(n)$ is the spectrum density of pressure fluctuations in time, $\rho$ is the density of air, $U_o$ is the maximum value of mean velocity, and $d$ is the diameter of the cylinder.

2. The mean-square pressure at the wall varies as the fourth power of the mean velocity at the center of the pipe.

3. The ratio of the root-mean-square pressure at the wall to the free-stream dynamic pressure is a constant (0.0078).

4. The mean-square sound pressure in the near field outside the cylinder varies as approximately the fifth power of the mean velocity at the center of the pipe.

5. The spectra of the pressure fluctuations in the external near-field scale with velocity.

6. The effect of increased wall thickness on the spectrum is to make the higher frequency part of the spectrum flatter. No definite similarity parameter, which would include the effect of wall thickness, was found.

7. The measurements indicate that present cylinder vibration theory is capable of predicting, quite accurately, the occurrence of natural frequencies in thin-walled cylinders under internal pressure when the cylinders are excited by turbulent flow.

California Institute of Technology,
Pasadena, Calif., August 18, 1959.

# APPENDIX

## NATURAL FREQUENCIES OF VIBRATION OF THIN-WALLED CYLINDERS UNDER INTERNAL PRESSURE

It is always difficult to determine precisely the date and author of a discovery. This seems to be the case with the work done on the vibrations of thin cylindrical shells. The subject is briefly touched upon in textbooks by Morse (ref. 19), Timoshenko (ref. 20), and others.

The first serious experimental work was carried out by Arnold and Warburton (refs. 21 and 22). However, in these experiments, the effects of internal pressure on the natural frequencies of vibration were not thoroughly investigated. Reissner (ref. 23), Mirsky and Herrmann (ref. 24), Fung, Sechler, and Kaplan (ref. 25), and several others also worked on the general problem of vibrating cylindrical shells.

Reference 25 is the first serious work, both theoretical and experimental, on the effects of internal pressure on the natural frequencies of vibration. In the experiments conducted by Fung, Sechler, and Kaplan, the cylinders were excited by a sinusoidal sound wave. In the present work the cylinders were excited by means of turbulent pipe flow. In this case the pressure fluctuations at the wall were produced by velocity fluctuations throughout the pipe flow. The cylinders were excited by forces describable by a correlation function having a particular shape. It is probable that, as in Willmarth's case, the wall pressures are convected and lose their identity after being carried downstream over a certain distance. However, since no space-time correlation measurements of the wall pressure were made it is not certain whether this is true.

Measurements of the frequency spectra of the wall pressure have been made as shown in figure 10. From these measurements it is possible to calculate the autocorrelation function

$$\psi(\tau) = \int_0^\infty F(n)\cos(2\pi n\tau)\,dn$$

The theory of vibration of thin cylindrical shells under internal pressure is rather complicated; however, it is useful to consider the frequency equation which is an eigen value equation. This equation determines the various natural frequencies of vibration from the elastic properties and constraints of the cylinder.

For a simply supported thin-walled cylinder, the simplified frequency equation states that

$$\frac{\pi^2 d^2 \rho_s f^2}{E} = \frac{\lambda_c^4}{\left(l^2 + \lambda_c^2\right)^2} + \frac{1}{12}(1 - \sigma^2)\left(\frac{2\tilde{t}}{d}\right)^2 \left(l^2 + \lambda_c^2\right)^2 + \bar{n}_x \lambda_c^2 + \bar{n}_\varphi l^2 \ . \ . \ .$$

(A1)

The first term on the right-hand side of the equation describes the influence of stretching of the shell, and the second term, the influence of bending. The last two terms describe the influence of axial stress and hoop stress due to internal pressure, respectively. For a particular cylinder, equation (A1) states that the natural frequency $f$ is given by the following relation

$$f = f\left(m, l, p_d\right)$$

Consequently, if for a fixed mode shape $(m, l)$ one measures two values of the natural frequency $f$ at two values of the pressure difference across the wall $p_d$, then one can solve for $m$ and $l$.

In the present experimental investigation, the above-mentioned method was used to determine the natural frequencies of vibration of the various cylinders.

## Measurement of Natural Frequencies of Vibration

Considerable time was spent making the airflow acoustically clean. Therefore, when it became evident that very sharp peaks occurred at the lower frequencies of the power spectra, as shown in figure 11, it was suspected that these peaks were associated with the natural frequencies of vibration of the cylinder. It was also observed that the peaks shifted with the pressure difference across the cylinder wall.

Accordingly, it was decided to measure carefully the frequency of each peak in the spectrum. Because the dial readings at low frequencies were none too accurate on this model wave analyzer, the following experimental procedure was adopted. Each peak in the spectrum was carefully tuned to show maximum deflection on the wave analyzer meter. A signal from an oscillator was then fed into the wave analyzer. The frequency of the oscillator was adjusted to give maximum deflection on the wave analyzer meter. Finally, the oscillator frequency was read. The method is essentially a step-by-step frequency calibration of the wave analyzer for each peak in the spectrum. It is a cumbersome but accurate method.

The various resonant frequencies of each cylinder are plotted against the pressure difference across the wall at a station directly underneath the microphone. The results are shown in figure 17 for cylinders of wall thicknesses 0.0005, 0.001, 0.0015, and 0.0021 inch.

## Discussion

The power spectra of the pressure fluctuations measured outside the cylinder always exhibited at least three and sometimes as many as six peaks. The fifth and sixth resonance peaks, if they occurred, were usually weak and considerably damped which made an accurate measurement of them somewhat difficult. Accordingly, figure 17 shows only the dependence of the first three or four natural frequencies on the pressure difference across the wall. The accuracy of the measurement of the natural frequencies was considered good and well within ±2 percent.

The calculation of the corresponding theoretical natural frequencies was made with the aid of frequency equation (A1), which involves two assumptions, both needing clarification.

The first assumption is that the cylinder is "freely supported" in such a manner that the ends remain circular and that no restraint on the axial or tangential displacement is imposed at the ends. The latter is not satisfied in the experimental setup. The effect of axial and tangential constraint at the ends will be to raise the value of the natural frequencies by a few percent, particularly at the lower mode $m = 1$.

In addition it is assumed in the theory (ref. 25) that the pressure difference across the wall is uniform along the cylinder. Since in the experiment the cylinder contains turbulent pipe flow, a pressure gradient exists along the pipe. The pressure difference across the wall of the cylinder at the ends is within ±10 percent of the pressure difference across the wall at the microphone station. It is not known to what extent the pressure gradient affects the natural frequencies of vibration.

The term $\bar{n}_x\lambda_c^2$ in equation (A1) is associated with the axial tension due to internal pressure, but this contribution is small in the experiment. However, the influence of skin friction must be considered. Accordingly, an estimate was made of the tension in the wall due to skin friction. Its effect was found to be small. The value of the various terms in equation (A1) is shown in table I for a cylinder of wall thickness 0.0005 inch. Four modes of vibration were considered.

From the calculations it is apparent that most of the energy is associated with the hoop stress and stretching of the shell. Very little energy is absorbed by the axial tension and wall bending. It is also interesting to note that the $l = 0$ mode, if it is excited, occurs at a very high frequency, well above 15,000 cps. This is because it requires a considerable amount of energy to excite the cylinder in such a mode, all the energy being absorbed by the stretching of the shell.

It is important to note that the mode shapes were not independently measured. Consequently, the comparisons between experiment and theory as shown in figure 17 are for probable comparable modes. However, the comparisons were thought to be fairly good since a slightly different choice of mode parameters $(m,l)$ would have resulted in theoretical curves substantially different from the experimental ones. Furthermore, the microphone was located at the center of each cylinder. It would therefore favor detection of mode shapes having an odd value of $m$, and, as shown in figure 17, most of the mode shapes have an odd value of $m$.

It is possible that additional vibration modes may have been present; however, they were not detected by the microphone.

Finally it should be noted that the magnitude of the response at the lowest eigen frequency is not necessarily the largest; that is, a larger response may occur at an eigen frequency which is several times the lowest one.

## REFERENCES


1. Phillips, O. M.: Surface Noise From a Plane Turbulent Boundary Layer. Rep. no. 16,963/FM 2099, British A.R.C., Aug. 4, 1954.

2. Phillips, O. M.: On the Aerodynamic Surface Sound From a Plane Turbulent Boundary Layer. Proc. Roy. Soc. (London), ser. A, vol. 234, no. 1198, Feb. 21, 1956, pp. 327-335.

3. Curle, N.: The Influence of Solid Boundaries on Aerodynamic Sound. Proc. Roy. Soc. (London), ser. A., vol. 231, no. 1187, Sept. 20, 1955, pp. 505-514.

4. Willmarth, W. W.: Wall Pressure Fluctuations in a Turbulent Boundary Layer. NACA TN 4139, 1958.

5. Willmarth, W. W.: Space-Time Correlations of the Fluctuating Wall Pressure in a Turbulent Boundary Layer. Jour. Aero. Sci., vol. 25, no. 5, May 1958, pp. 335-336.

6. Einstein, H. A., and Li, H.: The Viscous Sublayer Along a Smooth Boundary. Proc. Paper 945, EM 2, Am. Soc. Civ. Eng., Jour. Eng. Mech. Div., vol. 82, Apr. 1956.

7. Willmarth, W. W.: A Small Barium Titanate Transducer for Aerodynamic or Acoustic Pressure Measurements. Rev. Sci. Inst., vol. 29, no. 3, Mar. 1958, pp. 218-222.

8. Corcos, G. M., and Liepmann, H. W.: On the Contribution of Turbulent Boundary Layers to the Noise Inside a Fuselage. NACA TM 1420, 1956.

9. Kraichnan, R. H.: Pressure Field Within Homogeneous Anisotropic Turbulence. Jour. Acous. Soc., Am., vol. 28, no. 1, Jan. 1956, pp. 64-72.

10. Kraichnan, R. H.: Pressure Fluctuations in Turbulent Flow Over a Flat Plate. Jour. Acous. Soc. Am., vol. 28, no. 3, May 1956, pp. 378-390.

11. Kraichnan, R. H.: Noise Transmission From Boundary Layer Pressure Fluctuations. Jour. Acous. Soc. Am., vol. 29, no. 1, Jan. 1957, pp. 65-80.

12. Ribner, H. S.: Boundary-Layer-Induced Noise in the Interior of Aircraft. UTIA Rep. No. 37, Inst. of Aerophysics, Univ. of Toronto, Apr. 1956.

13. Laufer, J.: The Structure of Turbulence in Fully Developed Pipe Flow. NACA Rep. 1174, 1954.

14. Liepmann, H. W.: On the Application of Statistical Concepts to the Buffeting Problem. Jour. Aero. Sci., vol. 19, no. 12, Dec. 1952, pp. 793-800, 822.

15. Liepmann, H. W.: Parameters for Use in Buffeting Flight Tests. Rep. No. SM-14631, Douglas Aircraft Co., Inc., Jan. 3, 1953.

16. Liepmann, H. W.: Aspects of the Turbulence Problem (Part I). Z.a.M.P., Bd. III, Heft 5/6, 1952, pp. 321-342.

17. Wiener, N.: The Fourier Integral. The Univ. Press (Cambridge), 1930, p. 150.

18. Wiener, N.: Extrapolation, Interpolation, and Smoothing of Stationary Time Series. John Wiley & Sons, Inc., 1950.

19. Morse, P. M.: Vibration and Sound. McGraw-Hill Book Co., Inc., second ed., 1948.

20. Timoshenko, S.: Theory of Plates and Shells. McGraw-Hill Book Co., Inc., 1940.

21. Arnold, R. N., and Warburton, G. B.: Flexural Vibrations of the Walls of Thin Cylindrical Shells Having Freely Supported Ends. Proc. Roy. Soc. (London), ser. A, vol. 197, no. 1049, June 7, 1949, p. 238.

22. Arnold, R. N., and Warburton, G. B.: The Flexural Vibrations of Thin Cylinders. Jour. and Proc. Inst. Mech. Eng. (London), vol. 167, no. 1, Dec. 1953, pp. 62-74.

23. Reissner, E.: Non-Linear Effects in Vibrations of Cylindrical Shells. Rep. No. AM5-6, Ramo-Wooldridge Corp., Aug. 1955.

24. Mirsky, I., and Herrmann, G.: Nonaxially Symmetric Motions of Cylindrical Shells. Jour. Acous. Soc. Am., vol. 29, no. 10, Oct. 1957, pp. 1116-1123.

25. Fung, Y. C., Sechler, E. E., and Kaplan, A.: On the Vibration of Thin Cylindrical Shells Under Internal Pressure. Jour. Aero. Sci., vol. 24, no. 9, Sept. 1957, pp. 650-660.

TABLE I.- MAGNITUDE OF TERMS IN FREQUENCY EQUATION[a] FOR MYLAR CYLINDER OF WALL THICKNESS 0.0005 INCH WITH $p = 0.24$ psi

| Mode | $\frac{\lambda_c^4}{\left(l^2 + \lambda_c^2\right)^2}$ | $\frac{1 - \sigma^2}{12}\left(\frac{2\tilde{t}}{d}\right)^2\left(l^2 + \lambda_c^2\right)^2$ | $\frac{\overline{N_x}\lambda_c^2}{E\tilde{t}}$ | $\frac{pdl^2}{2E\tilde{t}}$ |
|---|---|---|---|---|
| $m = 1$<br>$l = 1$ | $0.418 \times 10^{-3}$ | $0.0078 \times 10^{-5}$ | $0.984 \times 10^{-5}$ | $0.0436 \times 10^{-2}$ |
| $m = 1$<br>$l = 2$ | 0.0259 | 0.12 | 0.984 | 0.174 |
| $m = 3$<br>$l = 2$ | 1.93 | 0.13 | 3.93 | 0.174 |
| $m = 5$<br>$l = 3$ | 2.87 | 0.67 | 8.78 | 0.392 |

[a]Frequency equation:

$$\frac{\pi^2 d^2 \rho_s f^2}{E} = \frac{\lambda_c^4}{\left(l^2 + \lambda_c^2\right)^2} + \frac{1 - \sigma^2}{12}\left(\frac{2\tilde{t}}{d}\right)^2\left(l^2 + \lambda_c^2\right)^2 + \frac{\overline{N_x}\lambda_c^2}{E\tilde{t}} + \frac{pdl^2}{2E\tilde{t}}$$

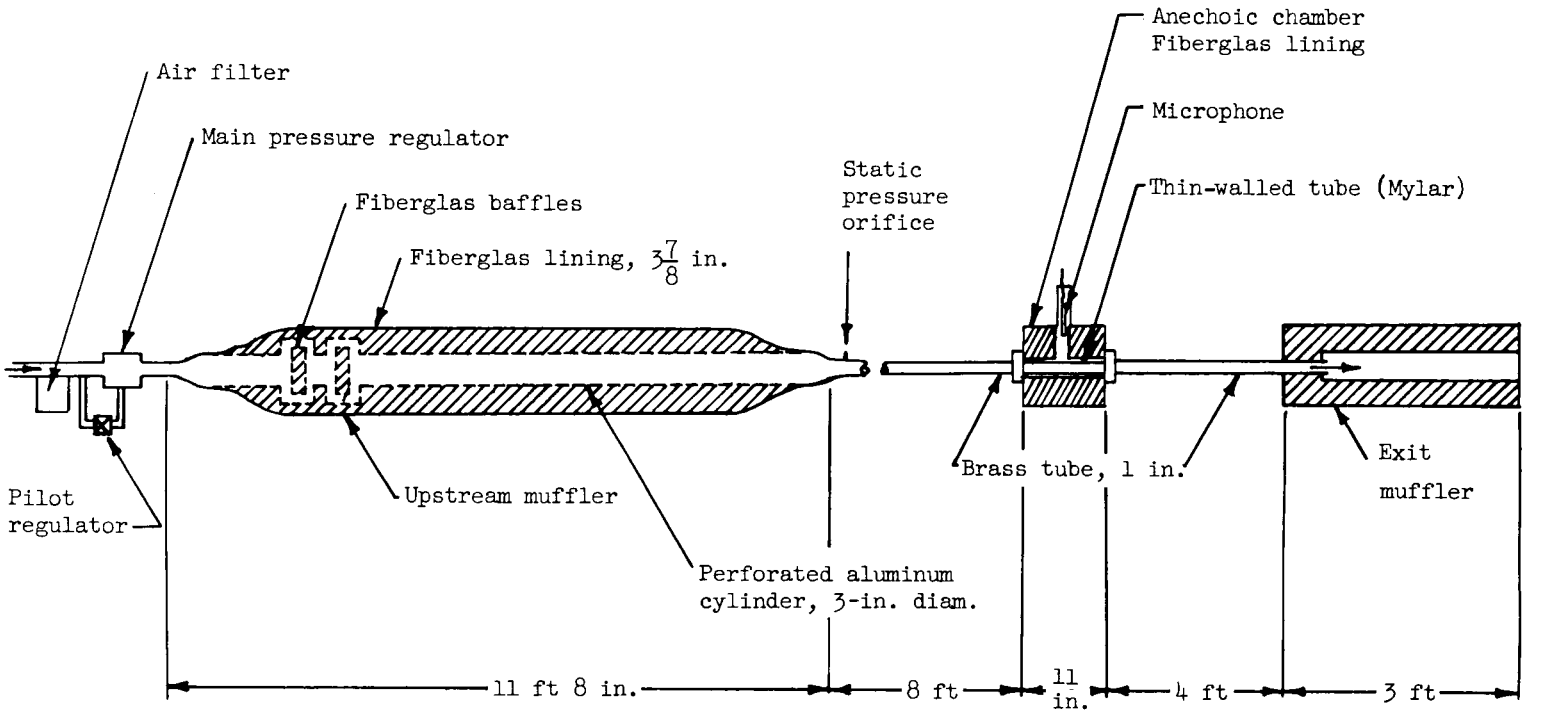


Figure 1.- Pipe flow apparatus.

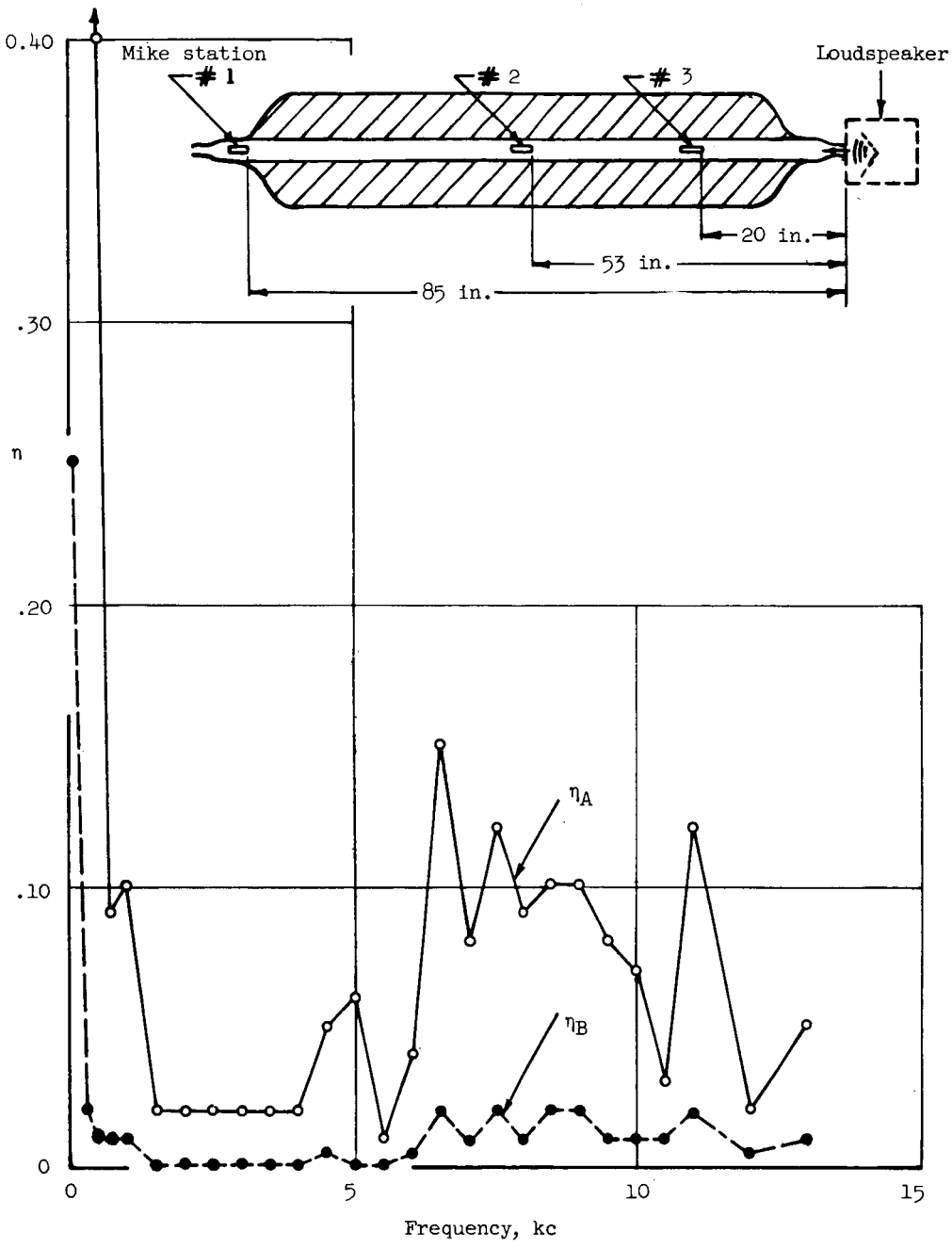


Figure 2.- Attenuation of sound in muffler.

$$\eta_A = \frac{\text{Sound level at station 1}}{\text{Sound level at station 2}};$$

$$\eta_B = \frac{\text{Sound level at station 1}}{\text{Sound level at station 3}}.$$

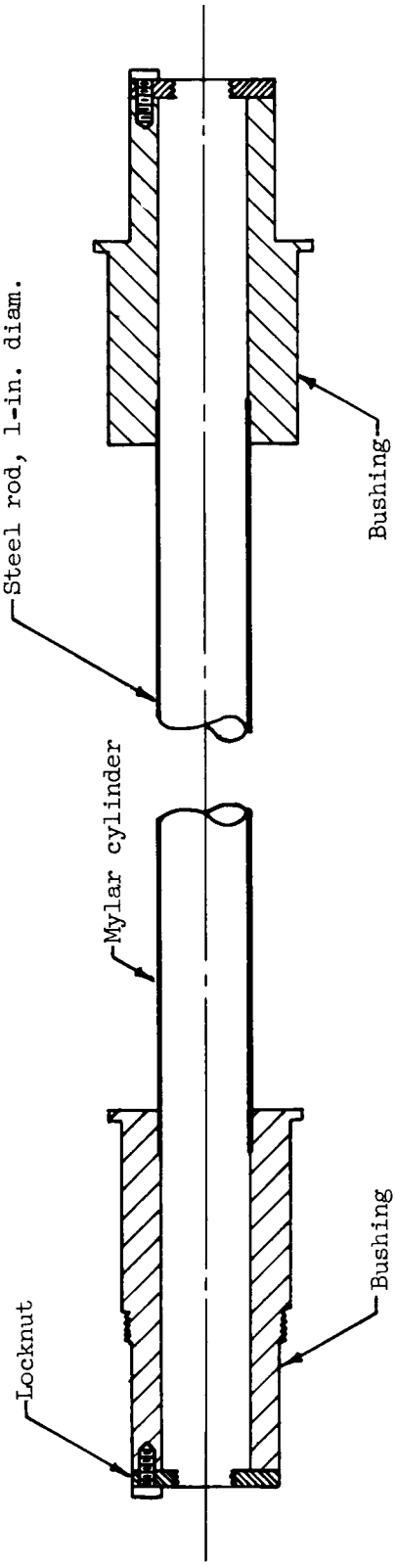


Figure 3.- Mylar cylinder assembly.

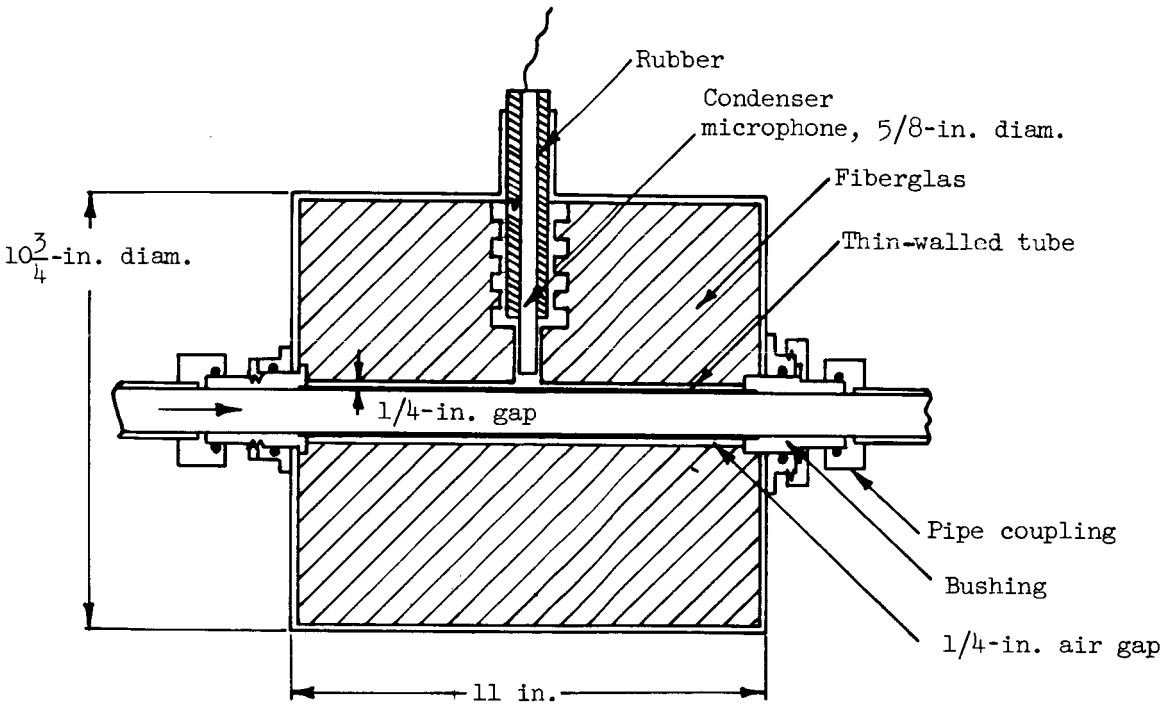


Figure 4.- Small-scale anechoic chamber.

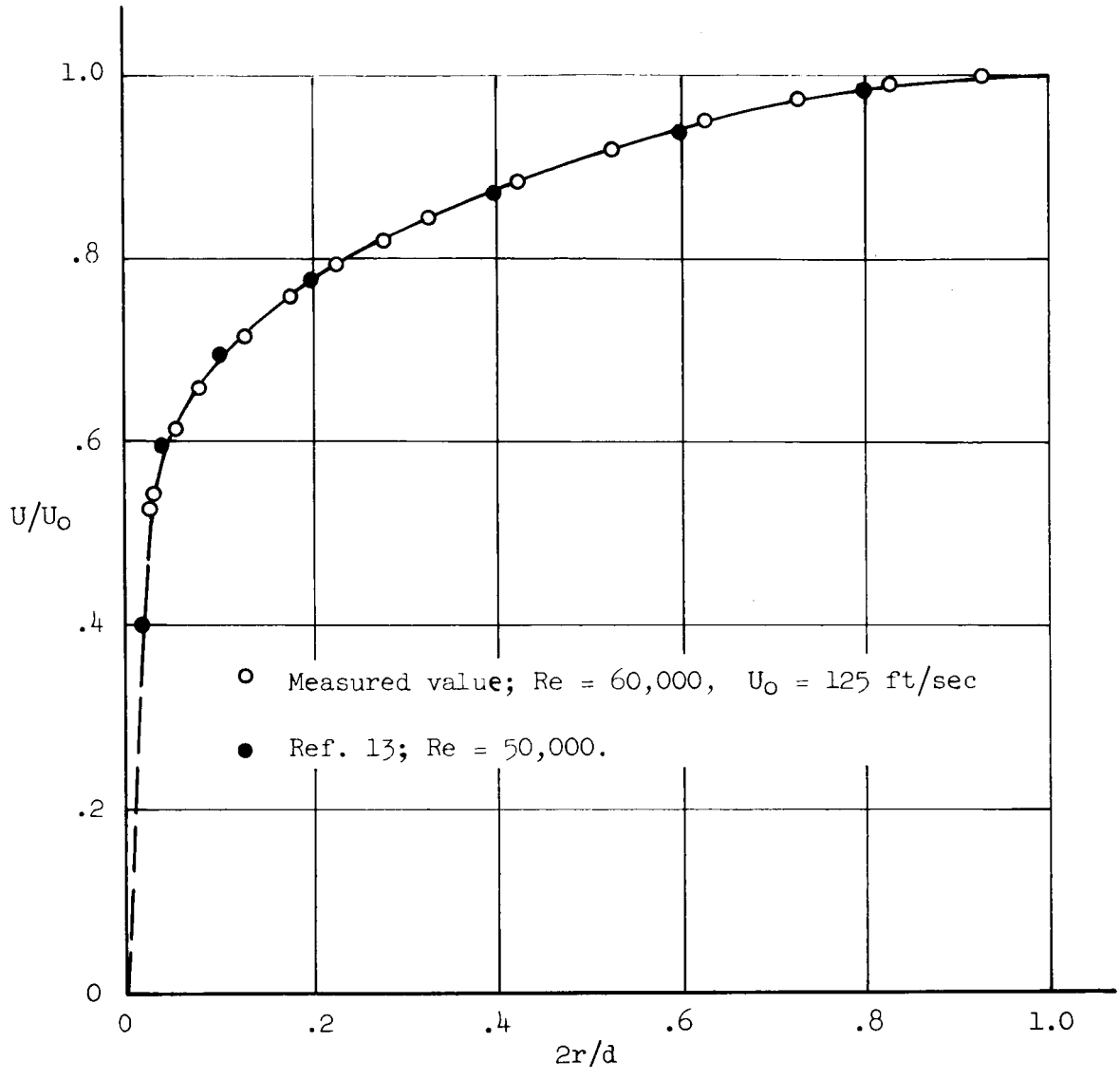


Figure 5.- Mean velocity distribution.

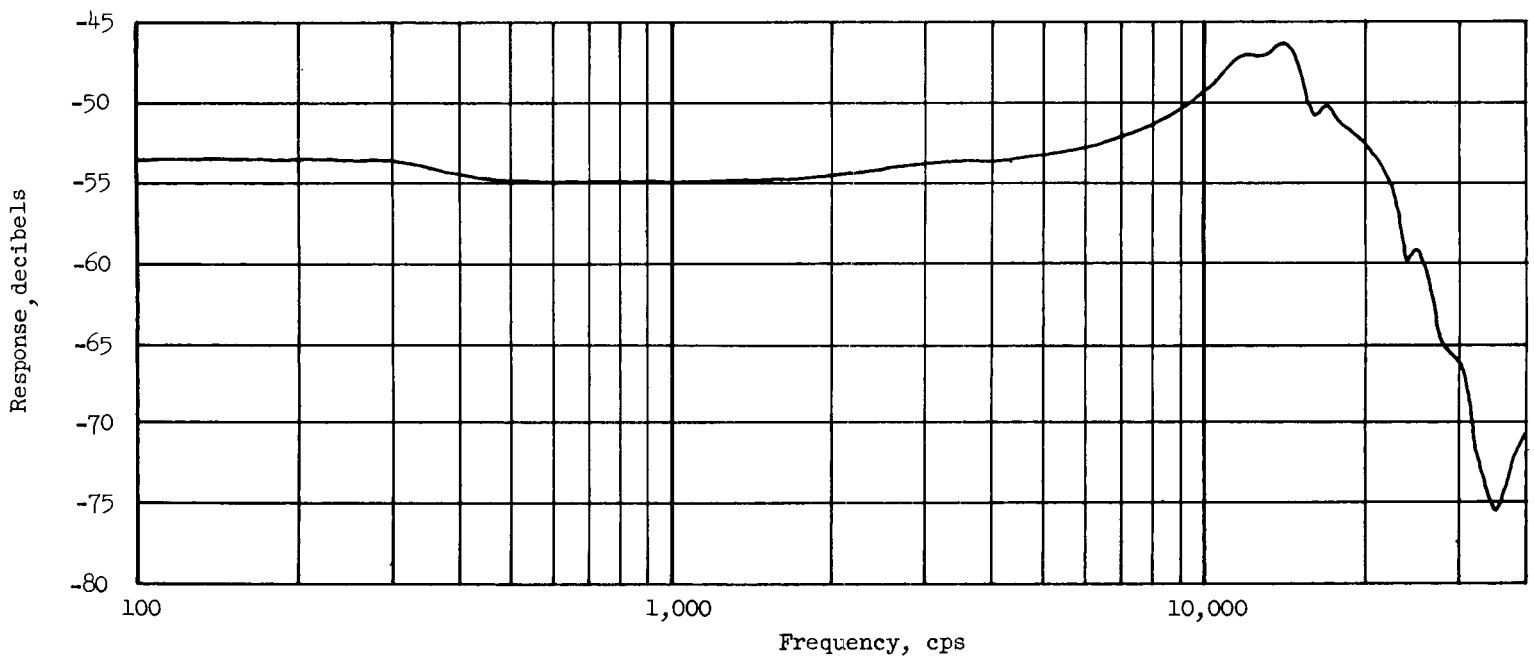


Figure 6.- Free-field open-circuit-calibration Altec 21-BR-150 microphone response at normal incidence. Reference base, 1 volt/dyne/square centimeter.

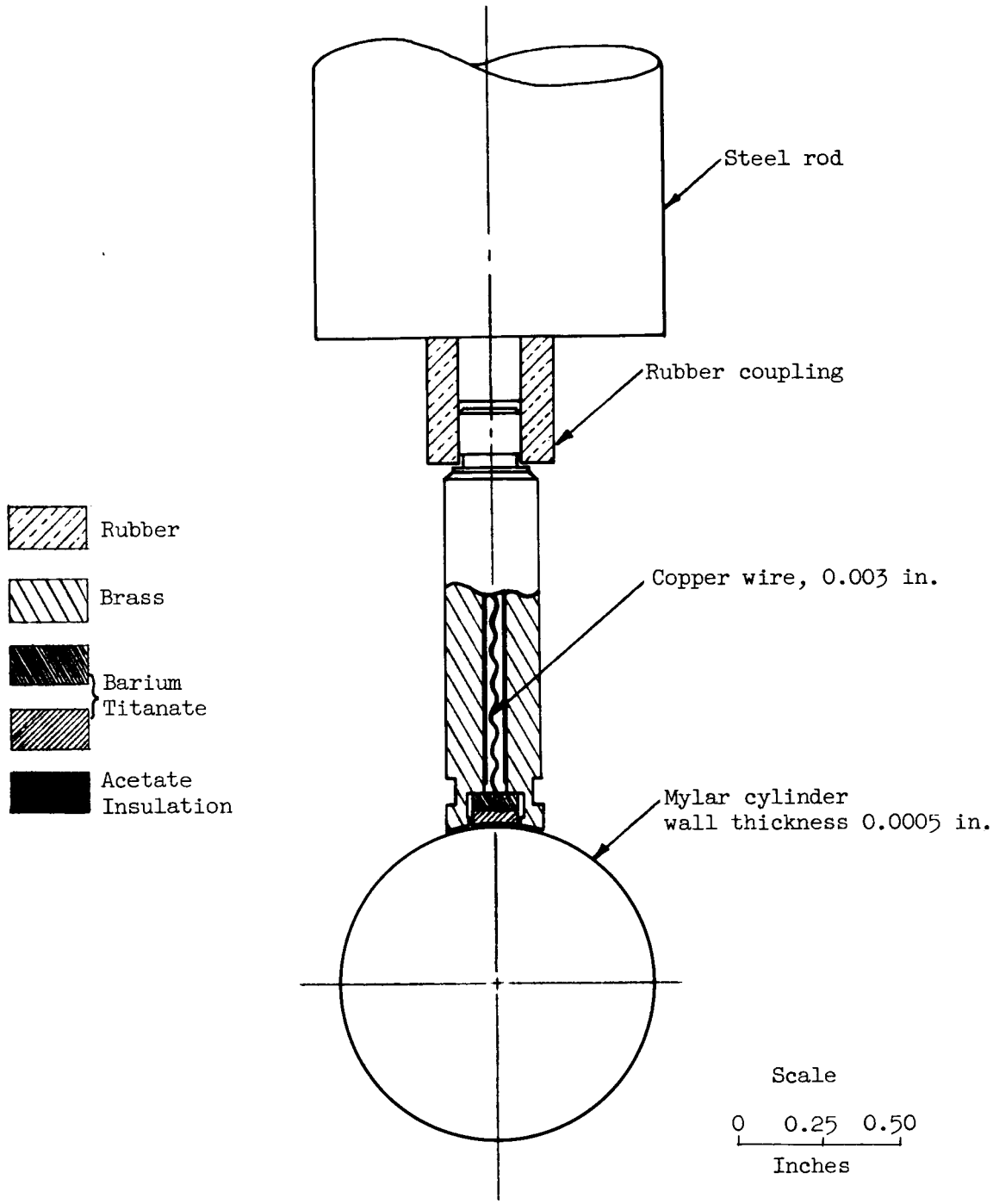


Figure 7.- Barium titanate pressure transducer assembly.

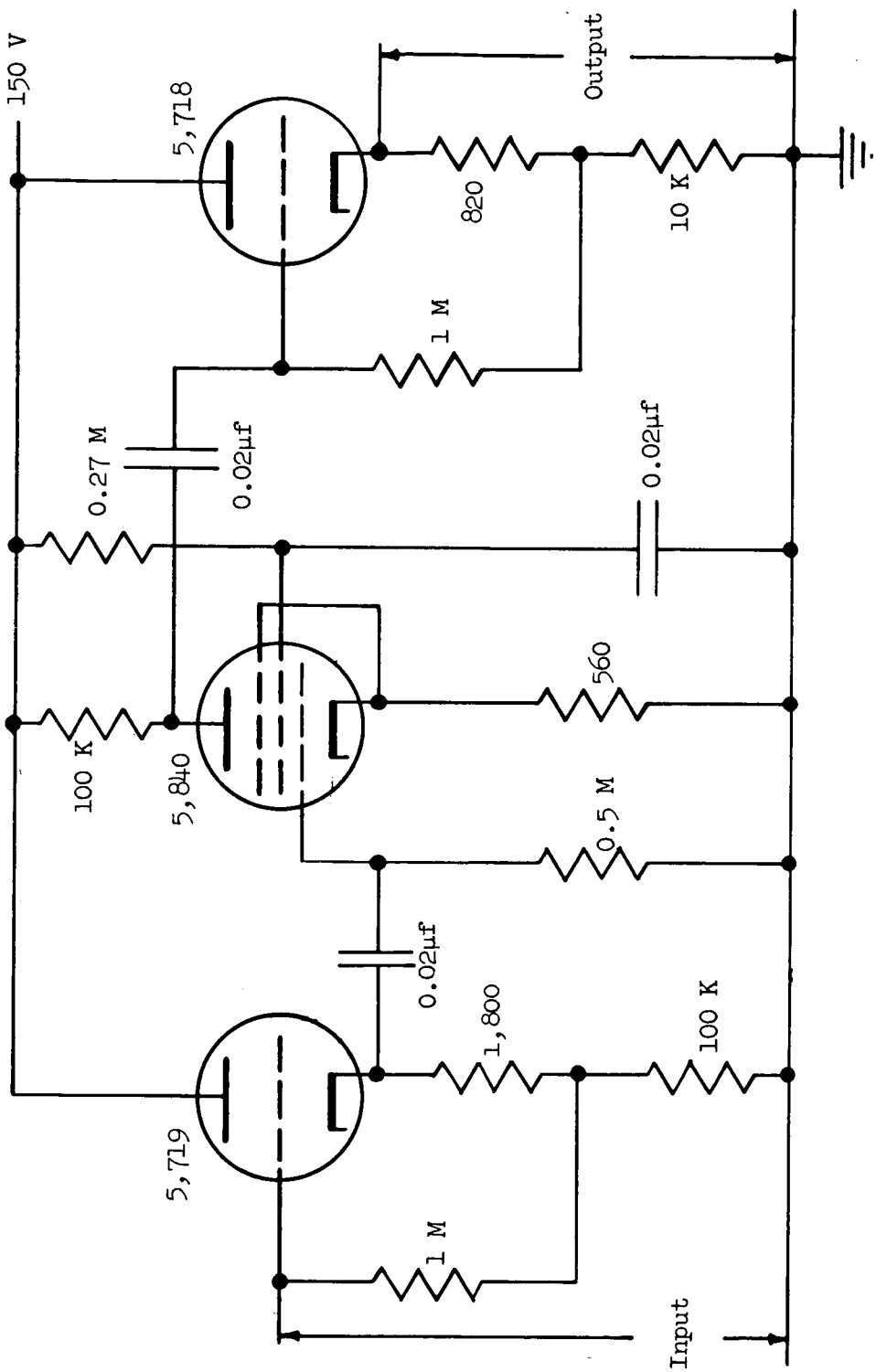


Figure 8.- Preamplifier circuit. All resistances are in ohms;
K = 1,000 ohms; M = 1,000,000 ohms.

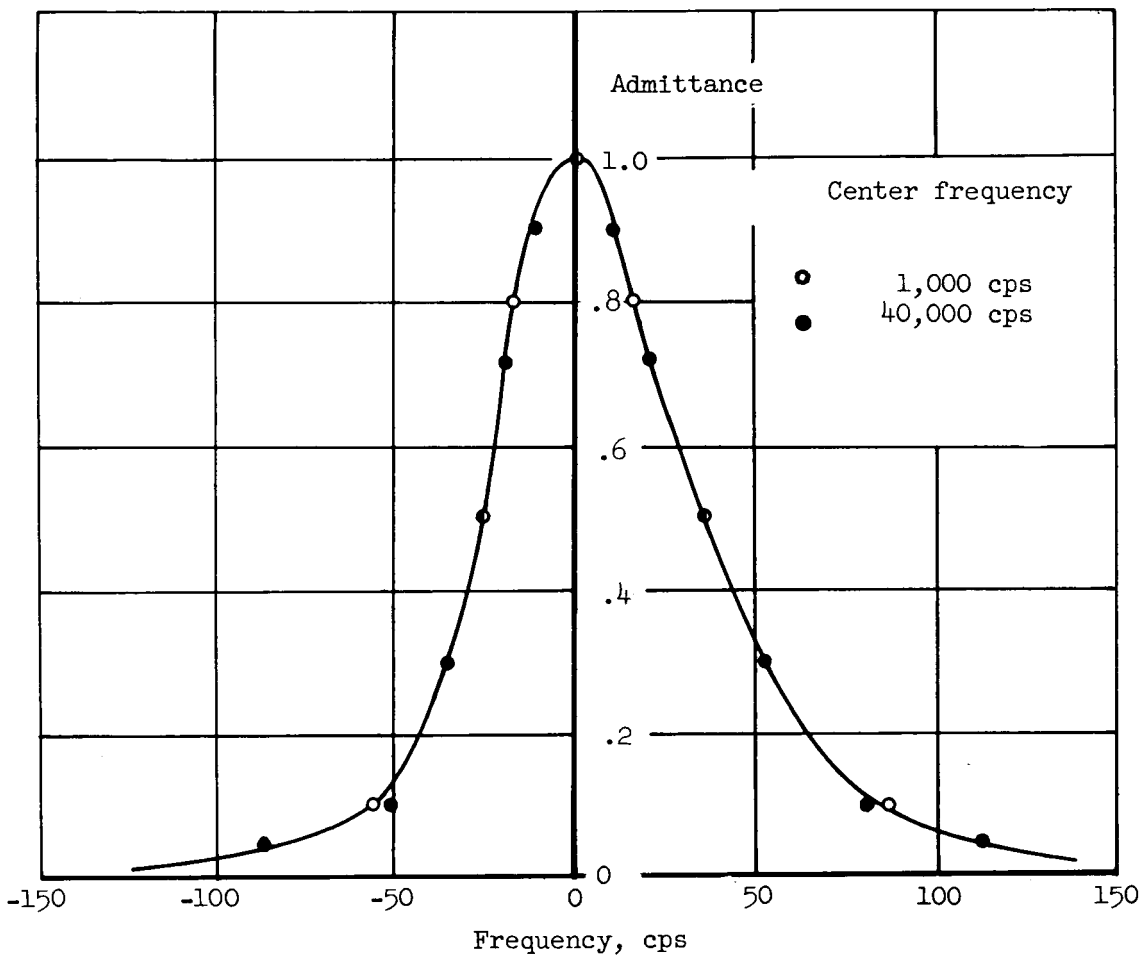


Figure 9.- Band-pass characteristics of Donner Model 21 wave analyzer.

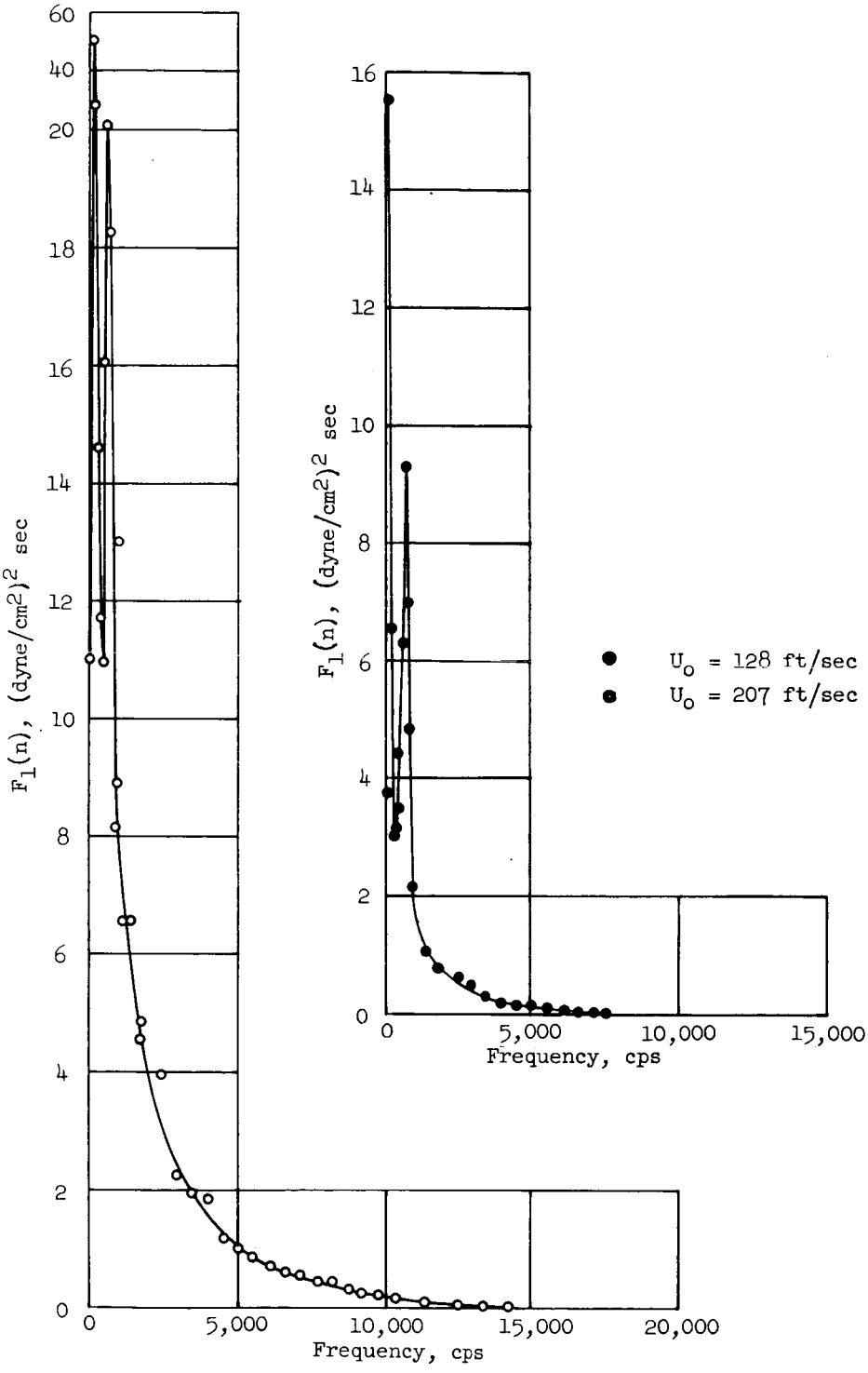


Figure 10.- Typical power spectra of pressure fluctuations at wall. Cylinder thickness, 0.0005 in.; diameter, 1 in.; station r/d = 1/2.

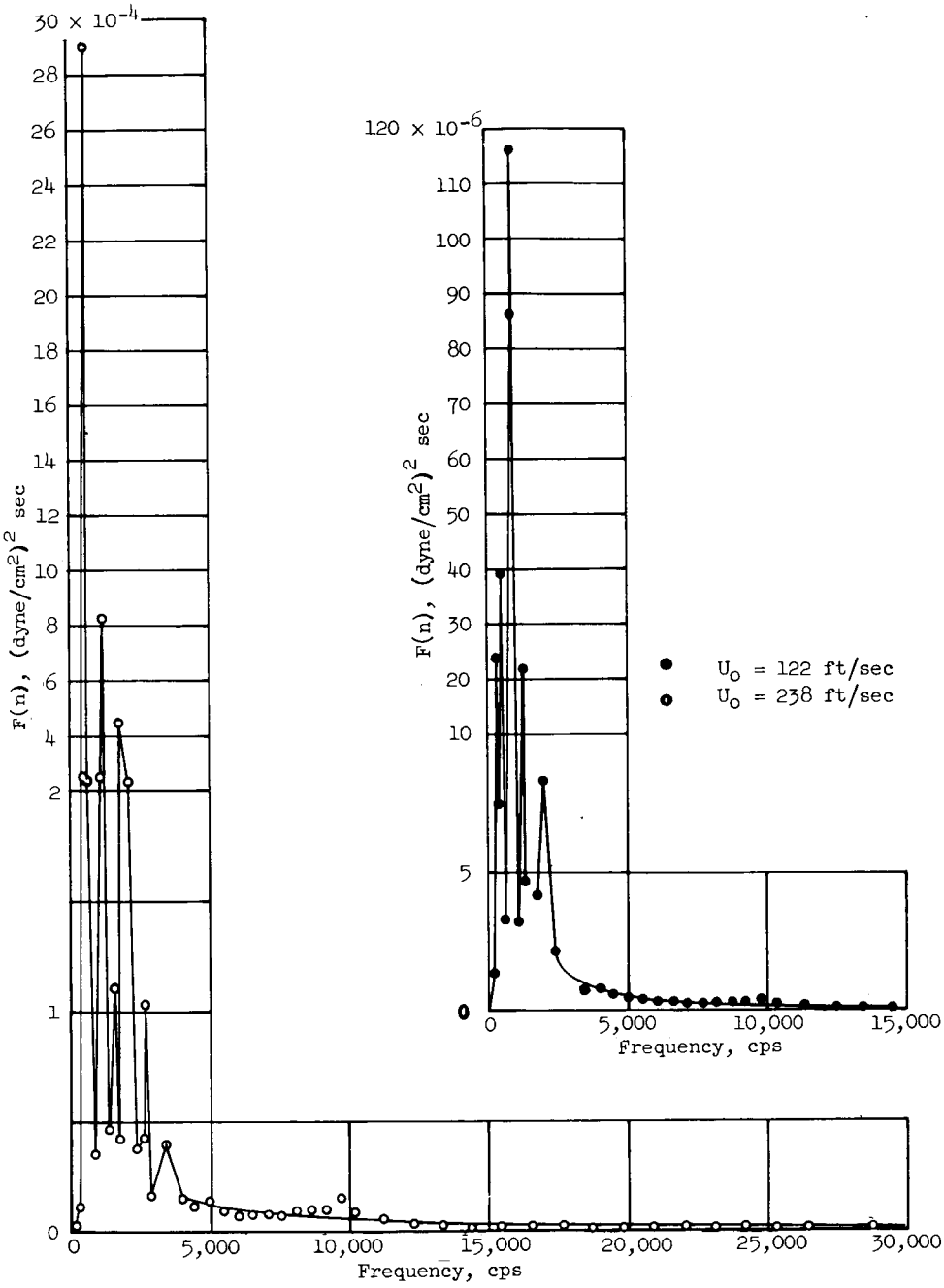


(a) Wall thickness, 0.0005 inch.

Figure 11.- Power spectra of external pressure for cylinder 1 inch in diameter at station r/d = 3/4.

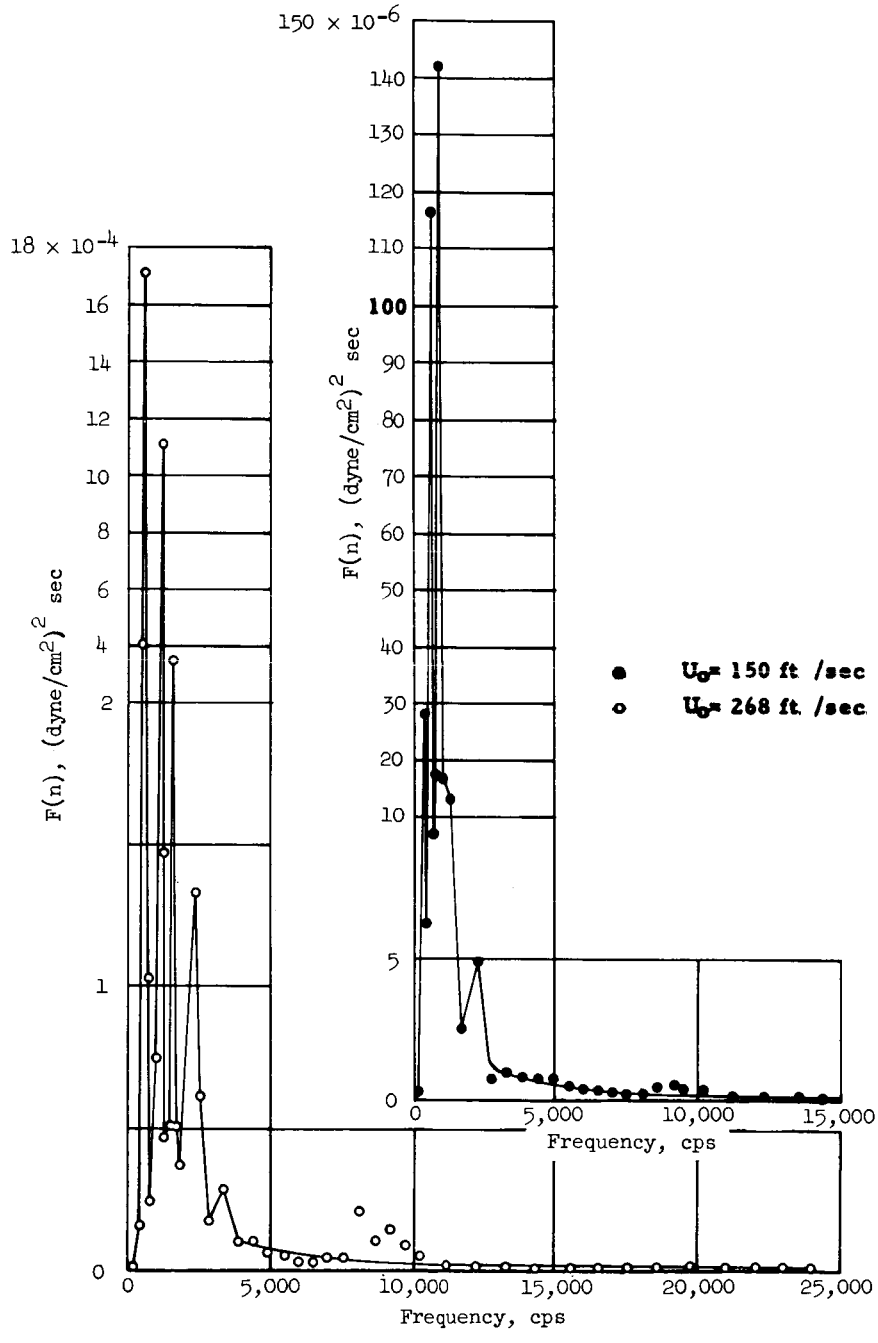


(b) Wall thickness, 0.001 inch.

Figure 11.- Concluded.

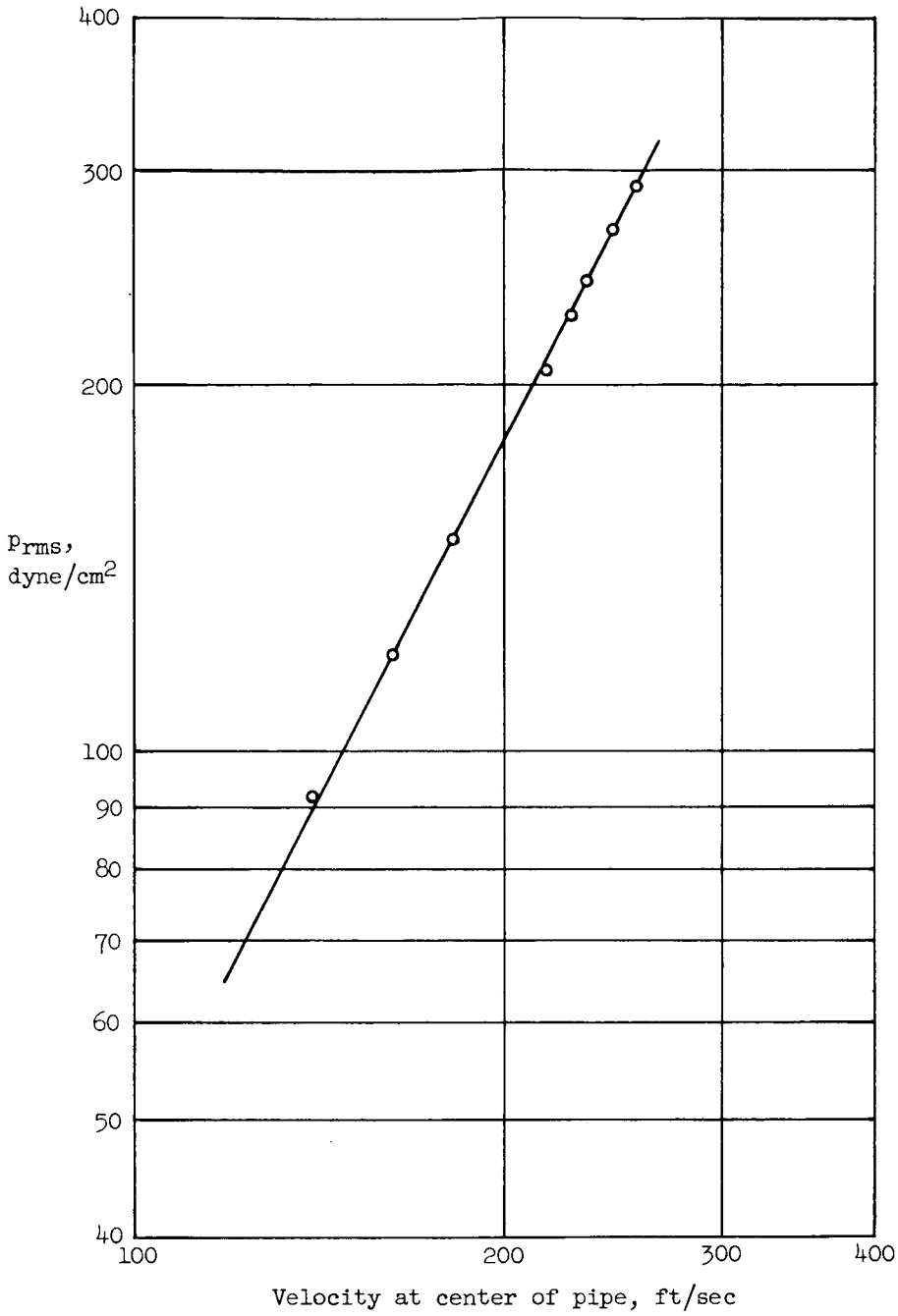


Figure 12.- Variation of root-mean-square pressure at wall with velocity. Cylinder thickness, 0.0005 in.; diameter, 1 in.; station r/d = 1/2.

Experimental result: $\overline{p^2} \propto U_o^{4.0}$; $\frac{P_{rms}}{q} = 0.0078$.

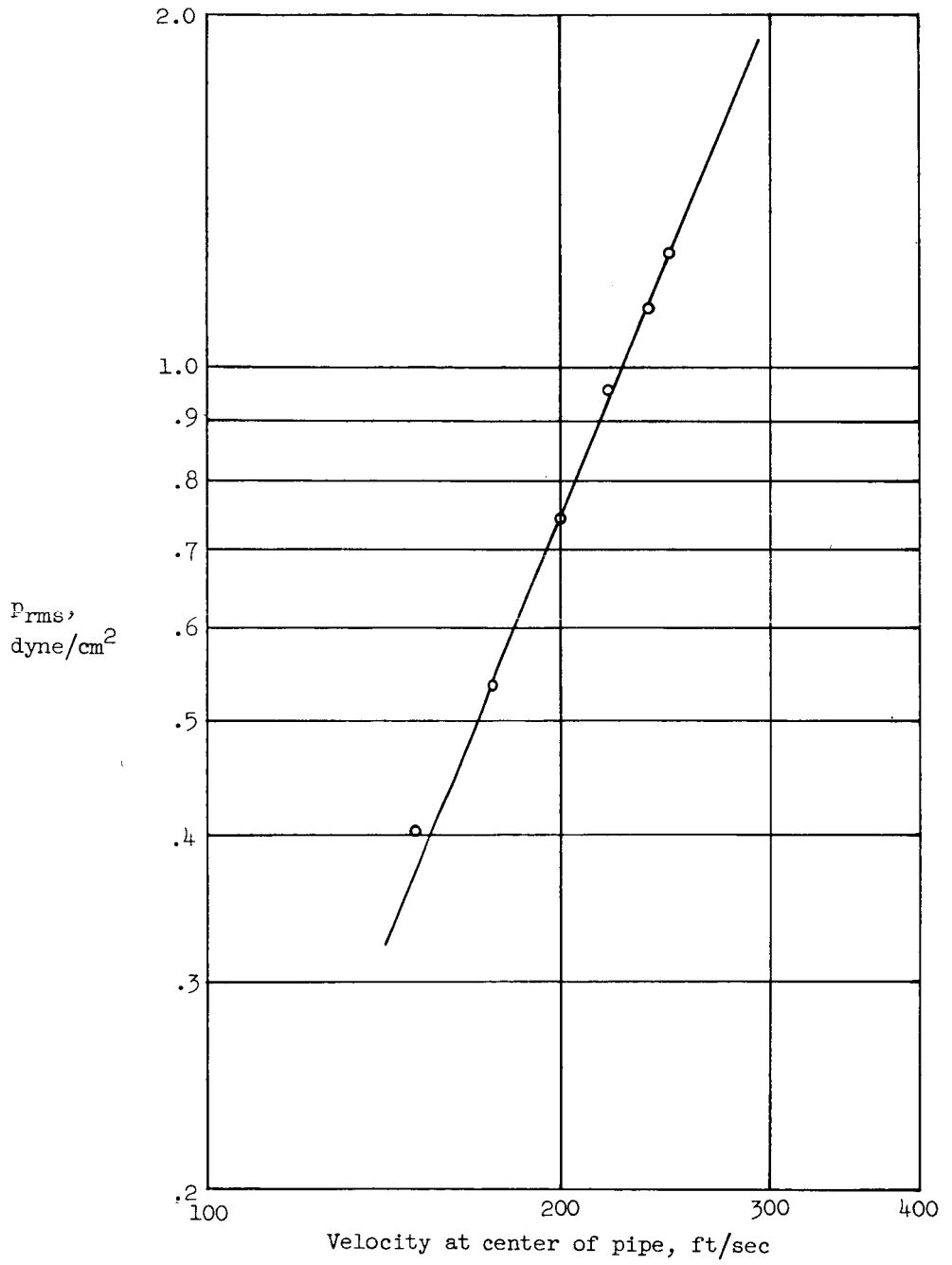


(a) Wall thickness, 0.0005 inch. Experimental result: $\overline{p^2} \propto U_o^{4.90}$.

Figure 13.- Variation of root-mean-square pressure at station $r/d = 3/4$ with velocity at center of pipe for cylinder 1 inch in diameter.

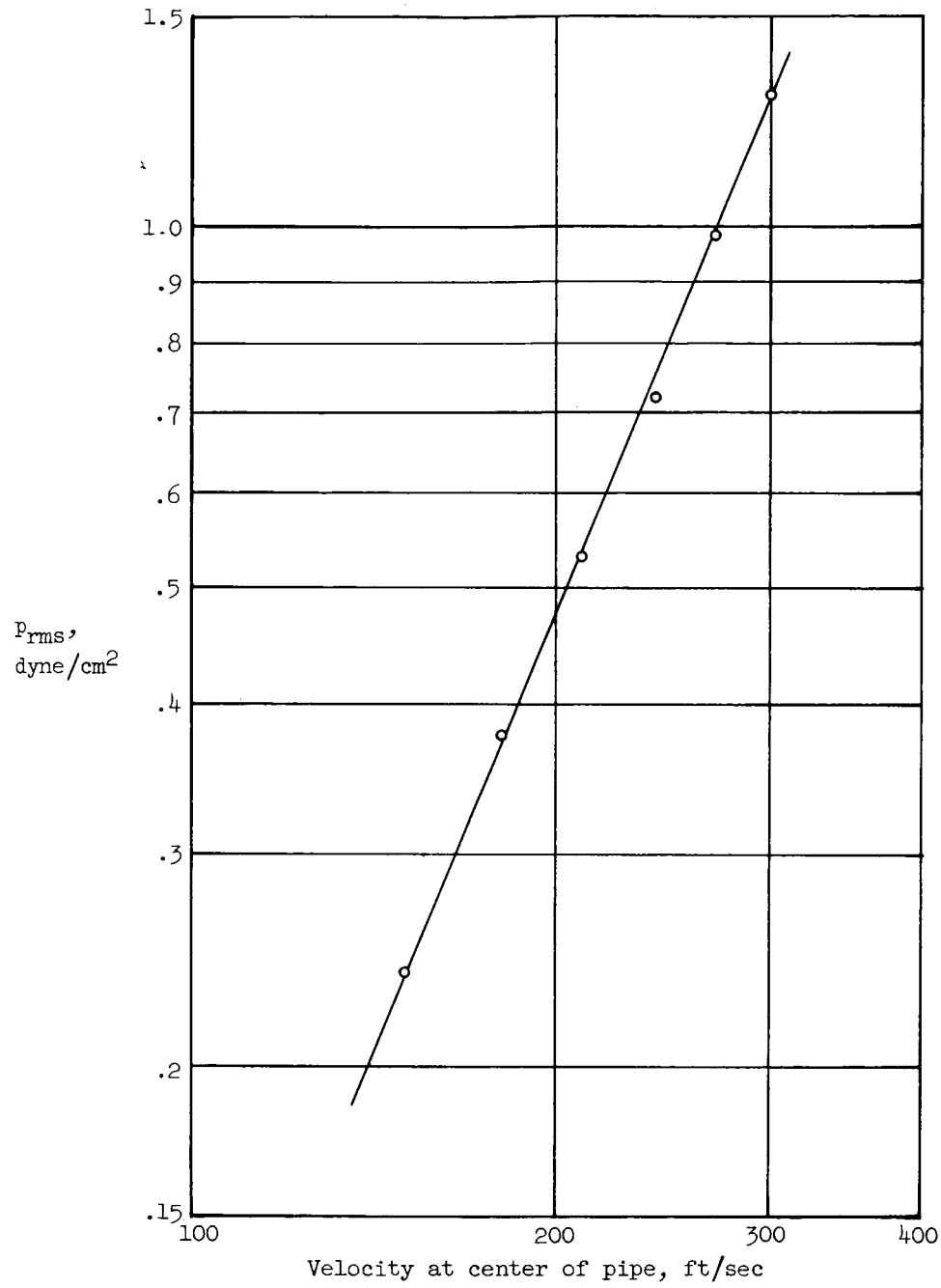


(b) Wall thickness, 0.001 inch. Experimental result: $\overline{p^2} \propto U_o^{4.92}$.

Figure 13.- Continued.

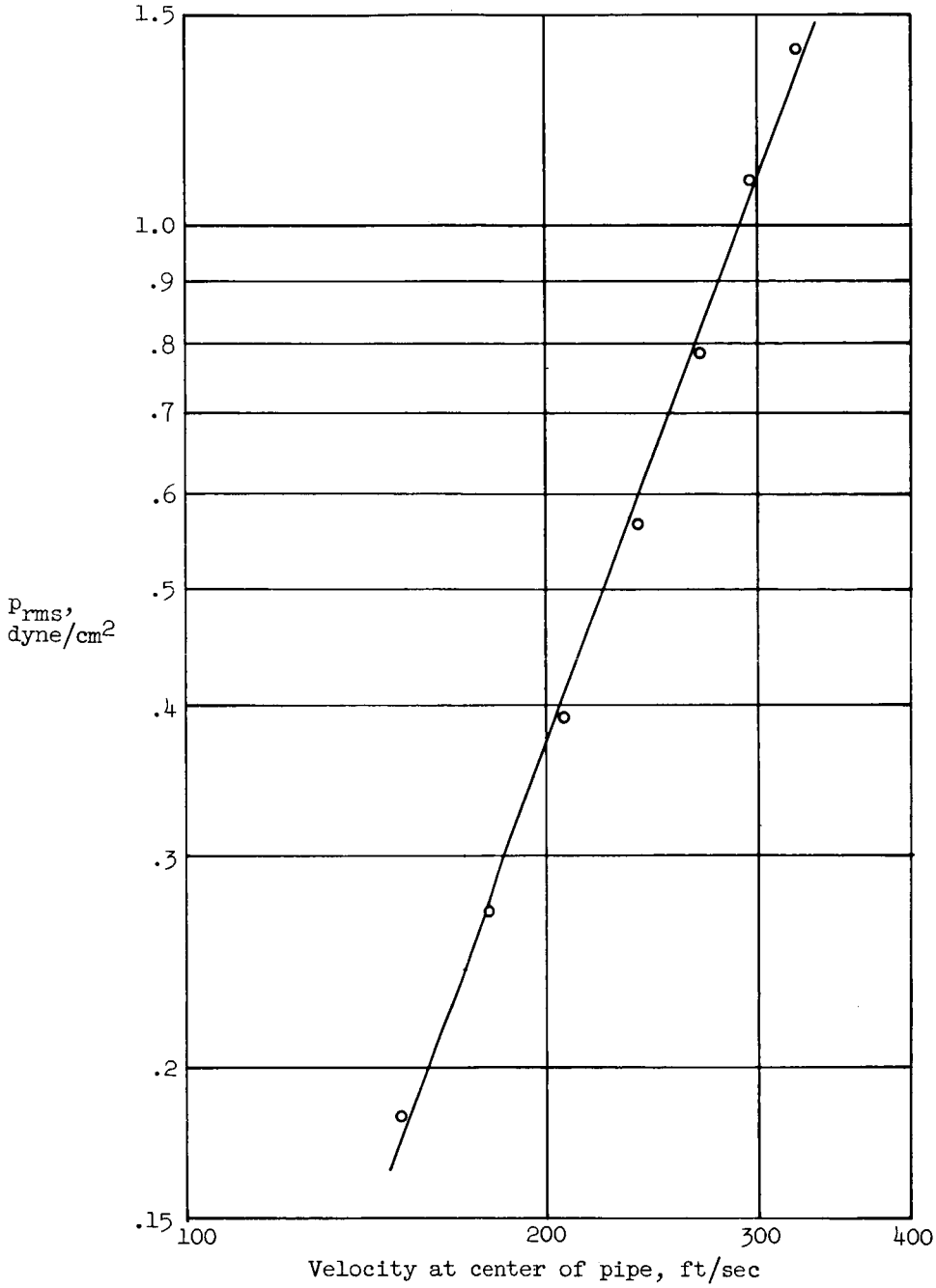


(c) Wall thickness, 0.0015 inch. Experimental result: $\overline{p^2} \propto U_o^{5.10}$.

Figure 13.- Continued.

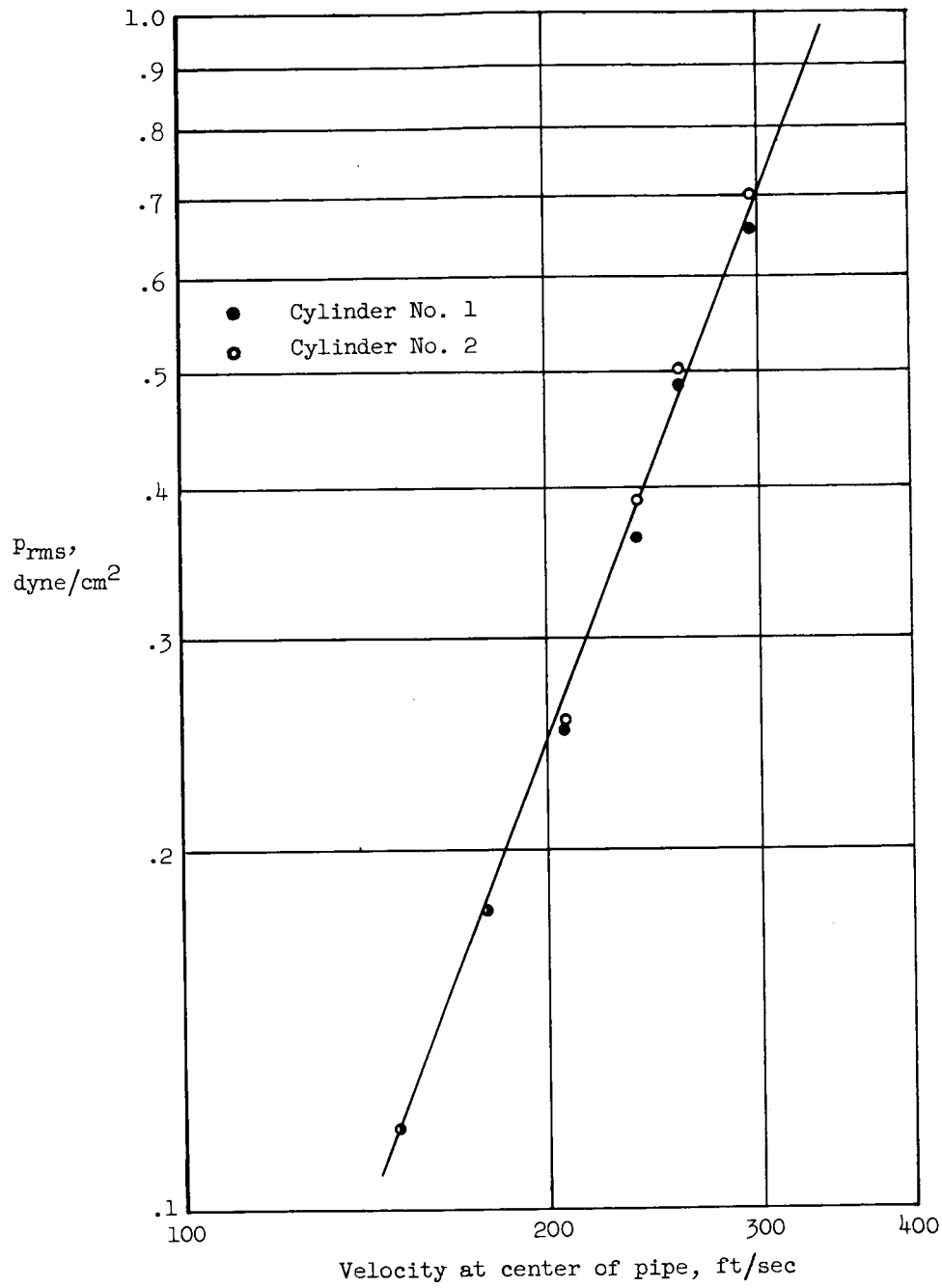


(d) Wall thickness, 0.0021 inch. Experimental result: $\overline{p^2} \propto U_o^{5.10}$.

Figure 13.- Concluded.

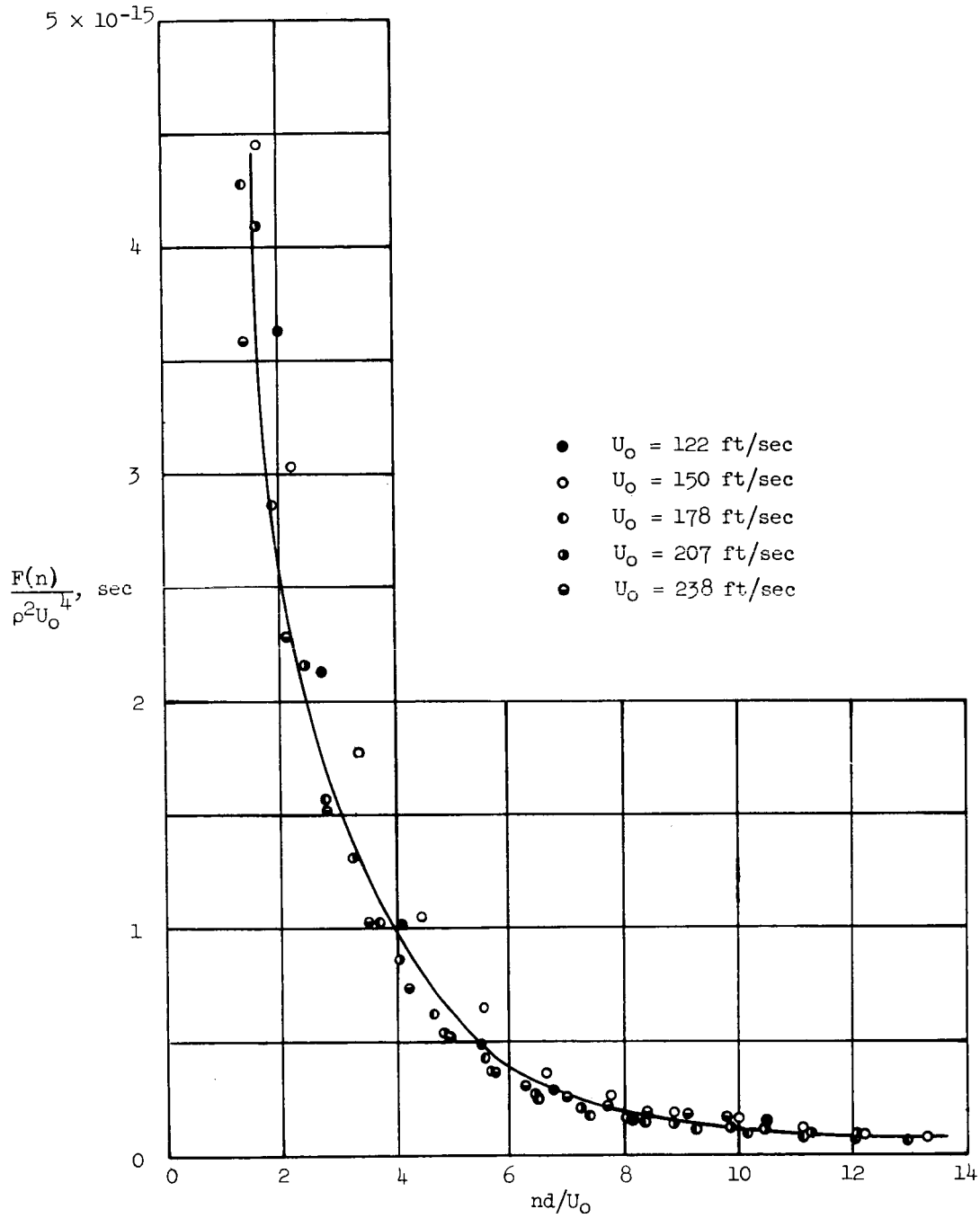


(a) Wall thickness, 0.0005 inch.

Figure 14.- Similarity of power spectra of p(t) for cylinder 1 inch in diameter at station r/d = 3/4.

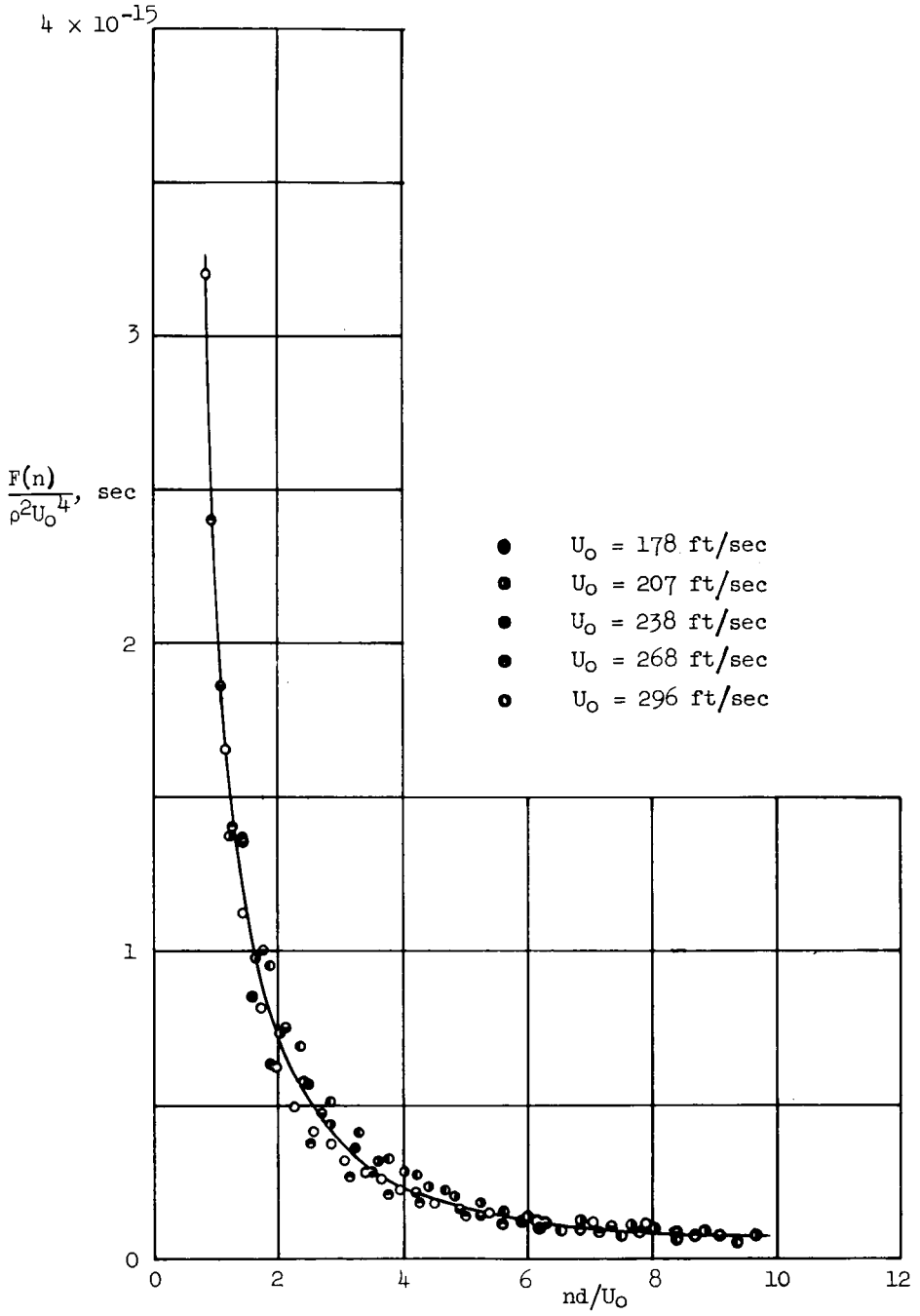


(b) Wall thickness, 0.001 inch.

Figure 14.- Continued.

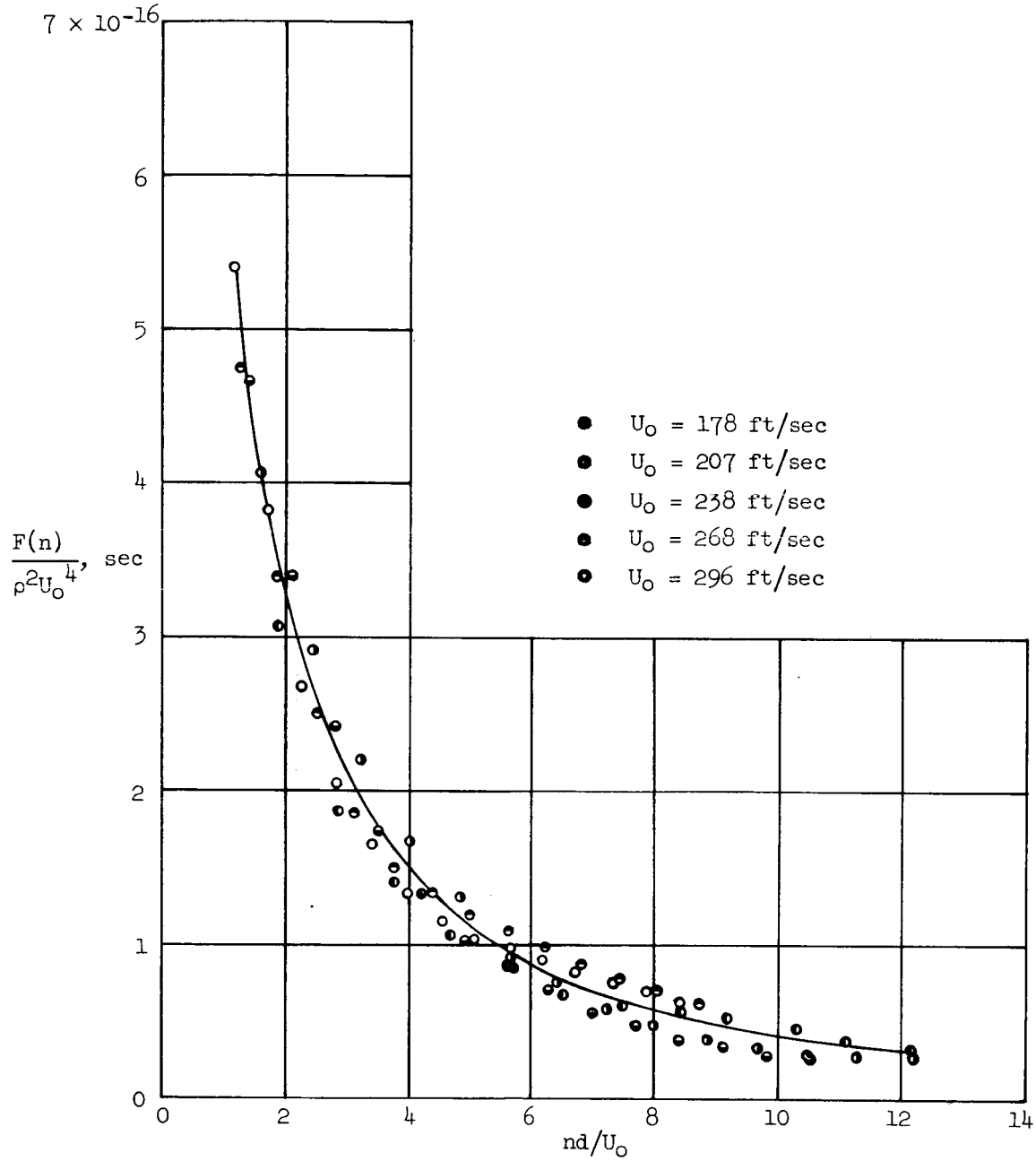


(c) Wall thickness, 0.0015 inch.

Figure 14.- Continued.

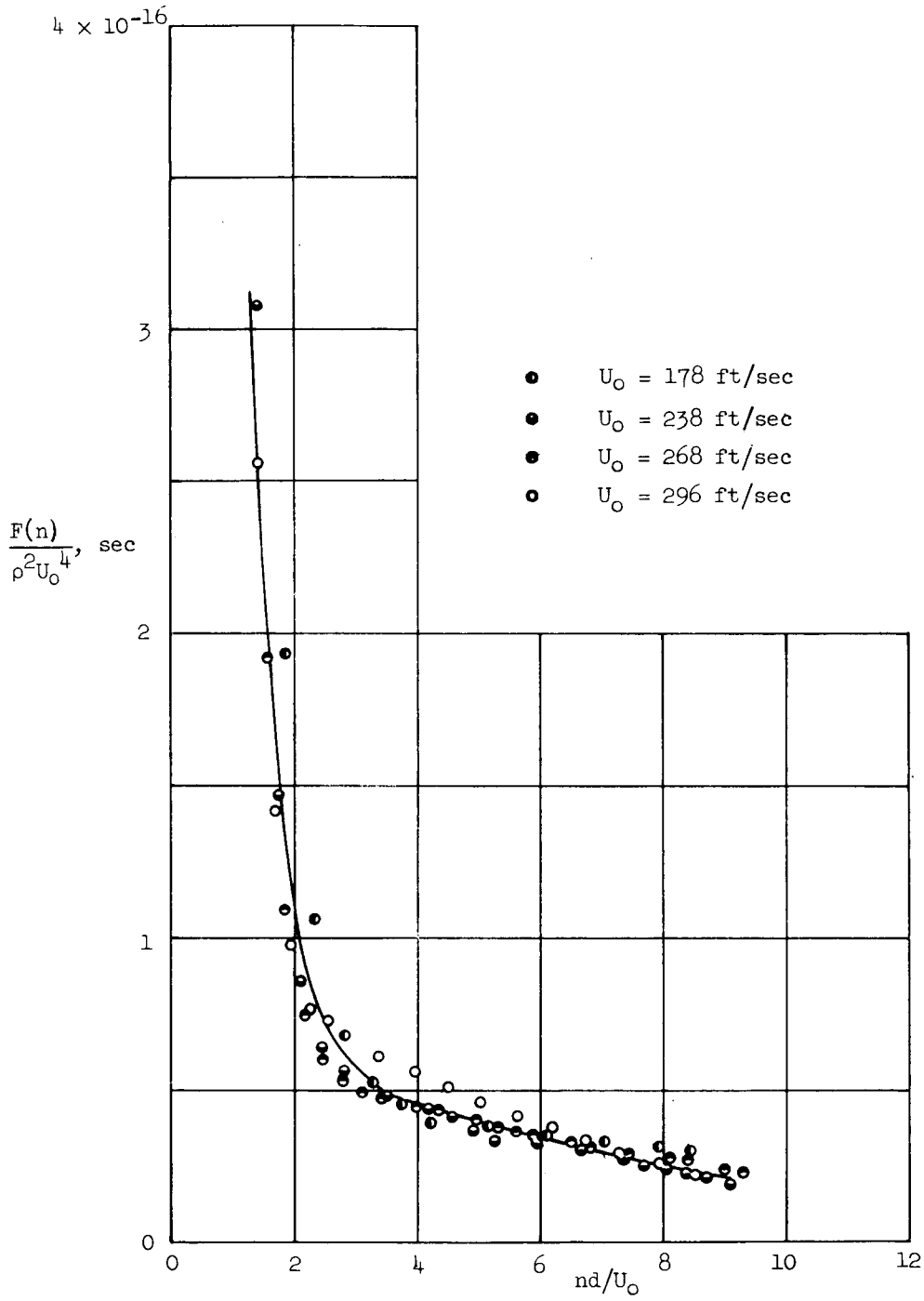


(d) Wall thickness, 0.0021 inch.

Figure 14.- Continued.

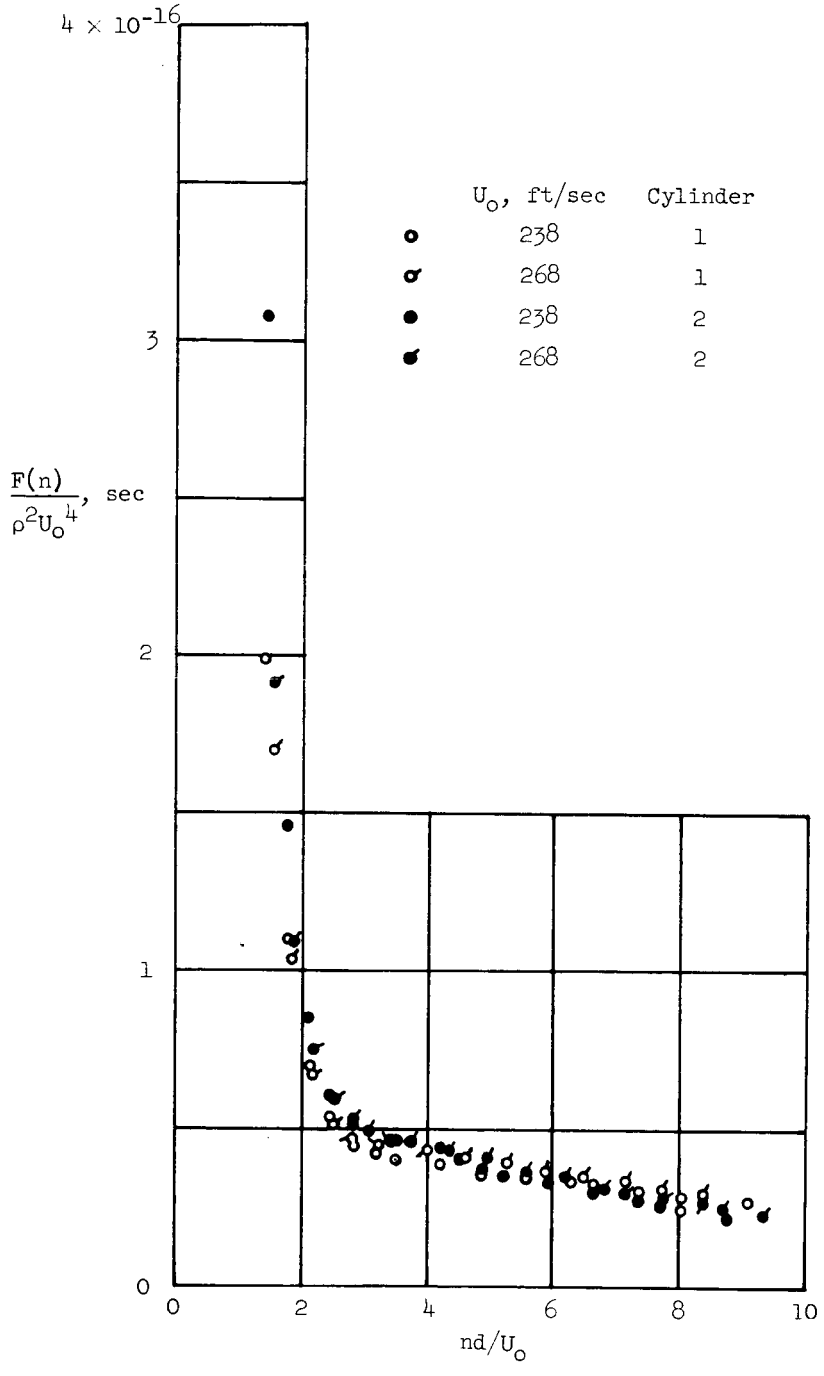


(e) Wall thickness, 0.0021 inch. Comparison of two cylinders of same wall thickness.

Figure 14.- Concluded.

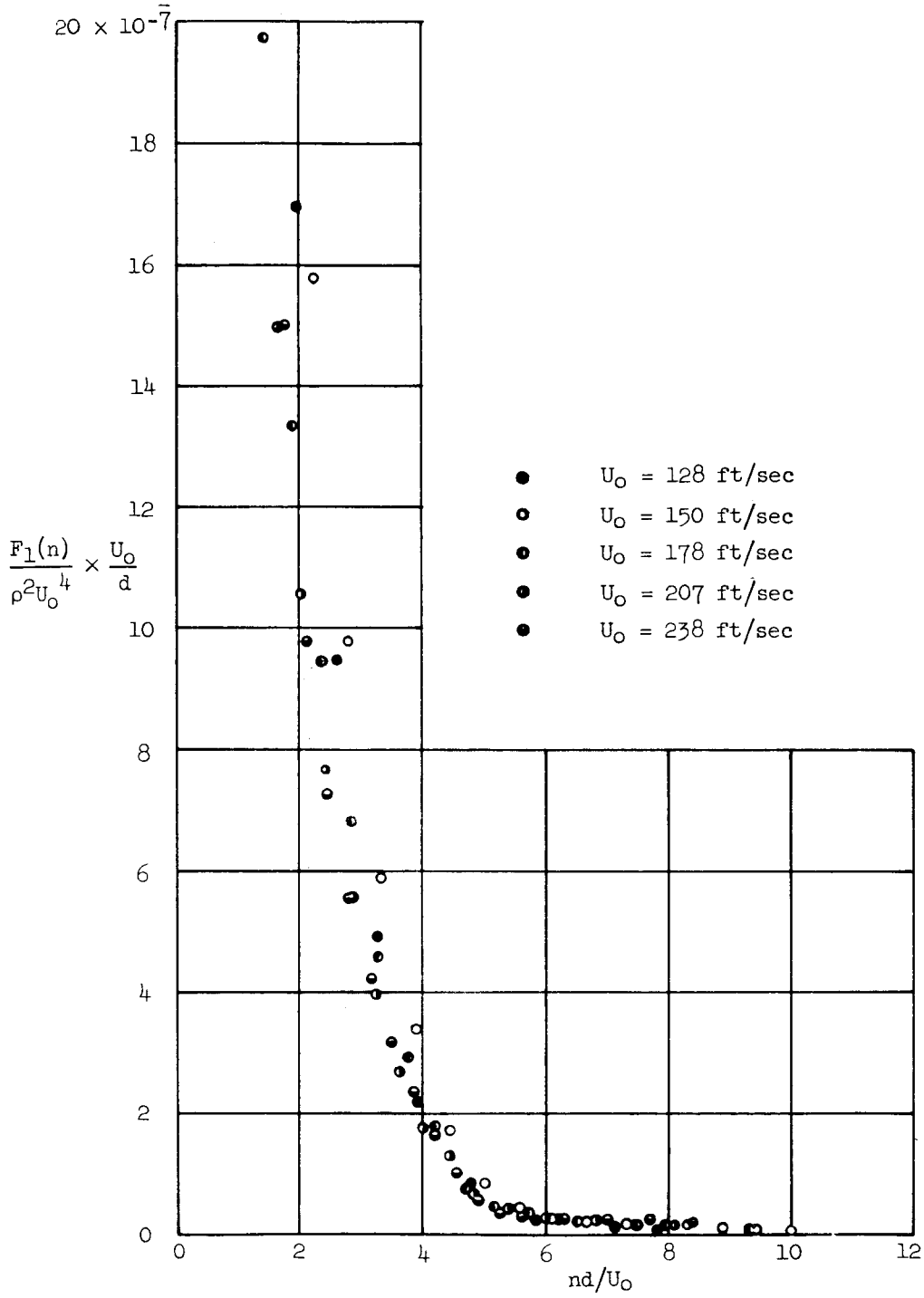


Figure 15.- Scaling of power spectra of p(t) with velocity. Cylinder thickness, 0.0005 inch; diameter, 1 inch; station r/d = 1/2.

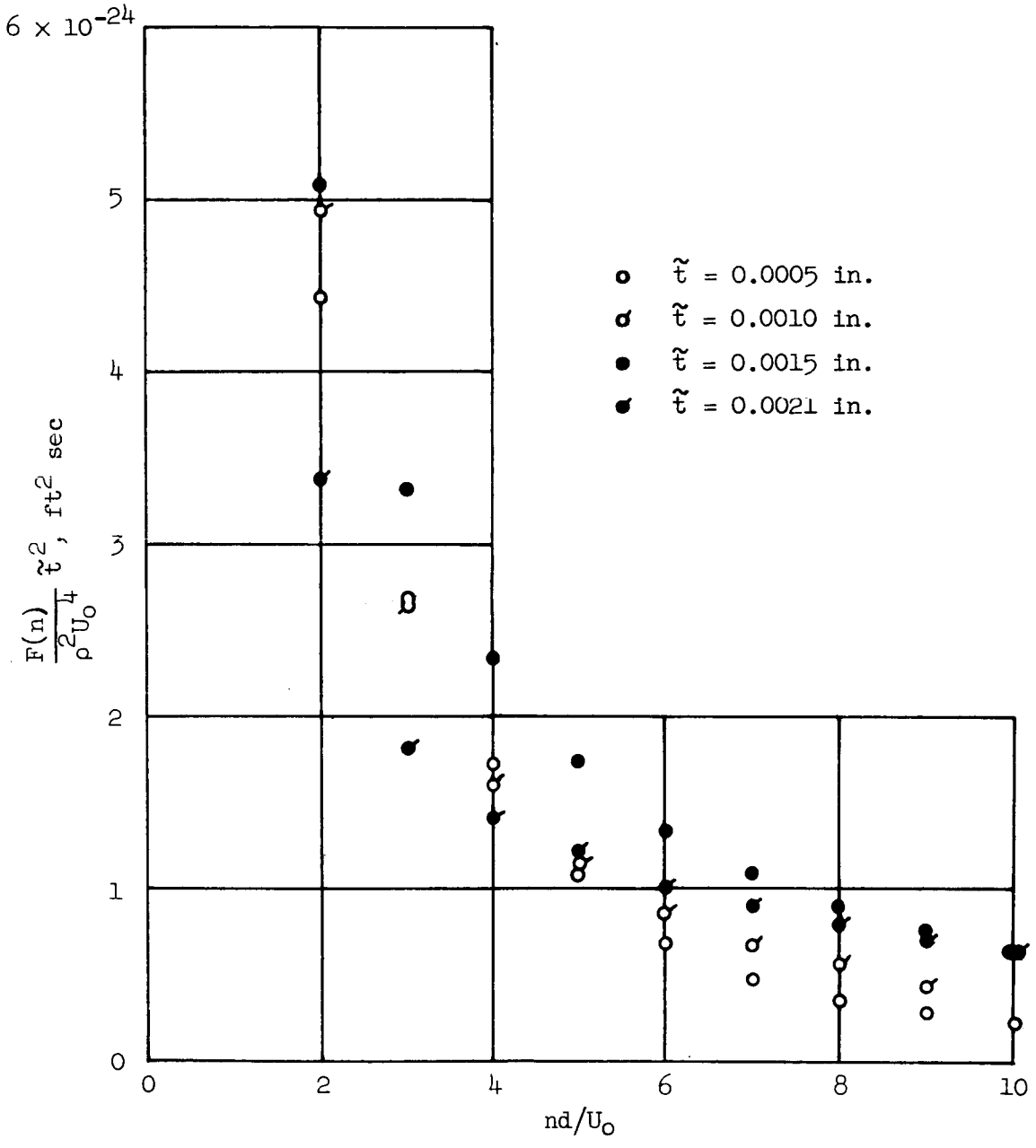


(a) Transmission loss proportional to mass of cylinder wall, effect of damping not included.

Figure 16.- Scaling of power spectra of p(t) with wall thickness.

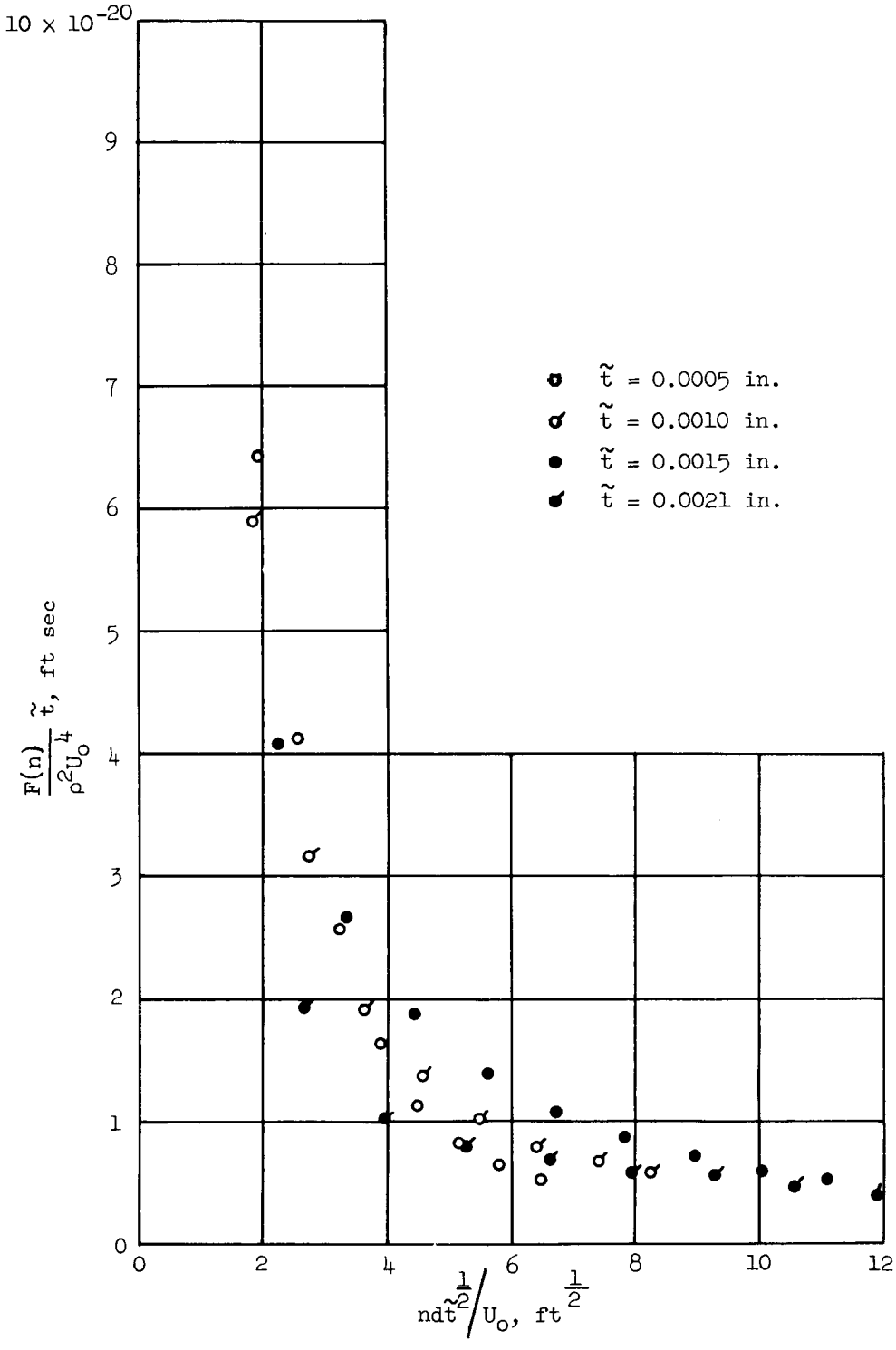


(b) Transmission loss proportional to mass of cylinder wall including effect of air damping.

Figure 16.- Concluded.

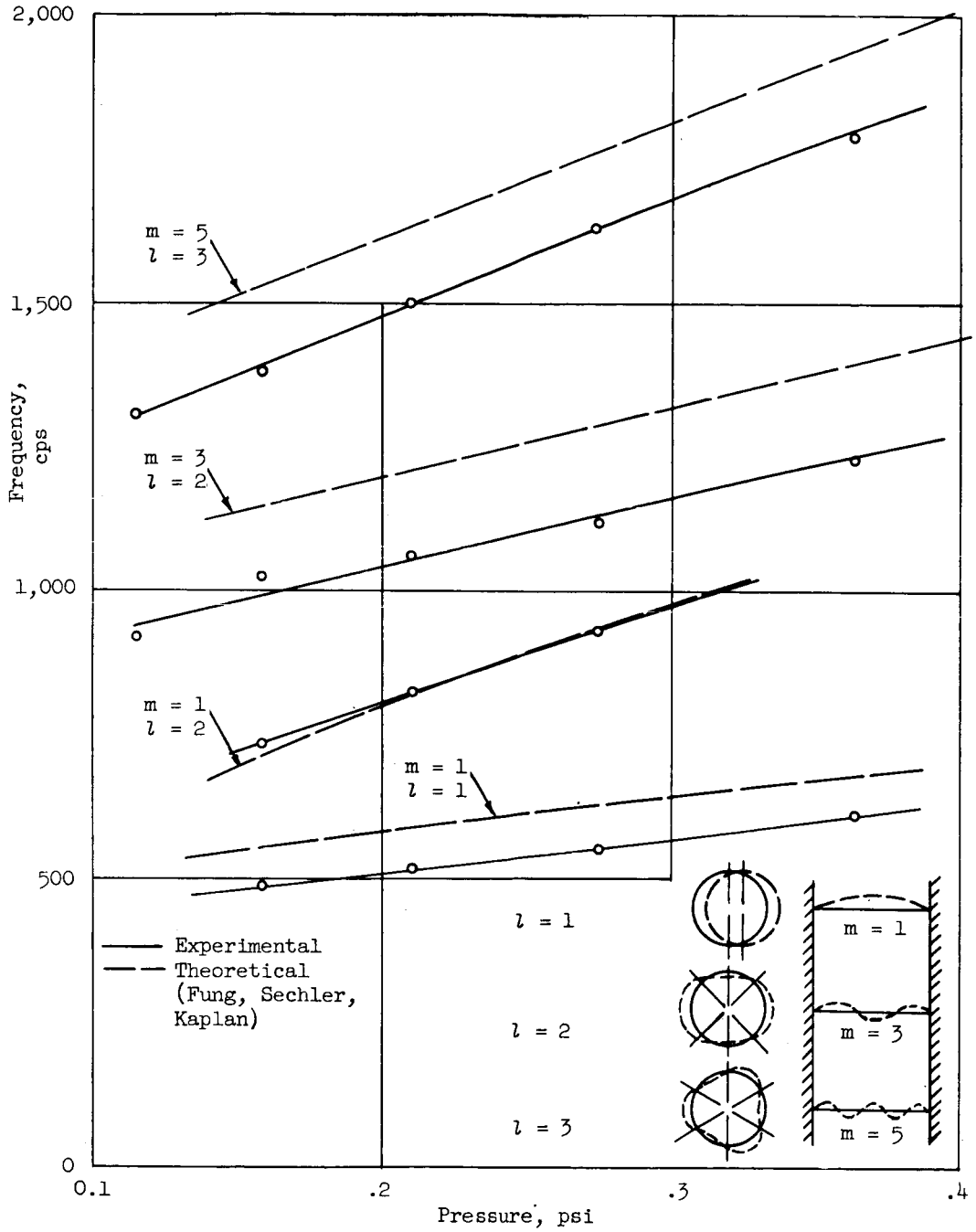


(a) Wall thickness, 0.0005 inch.

Figure 17.- Natural frequencies versus pressure difference across Mylar cylinder 1 inch in diameter and 11 inches long.

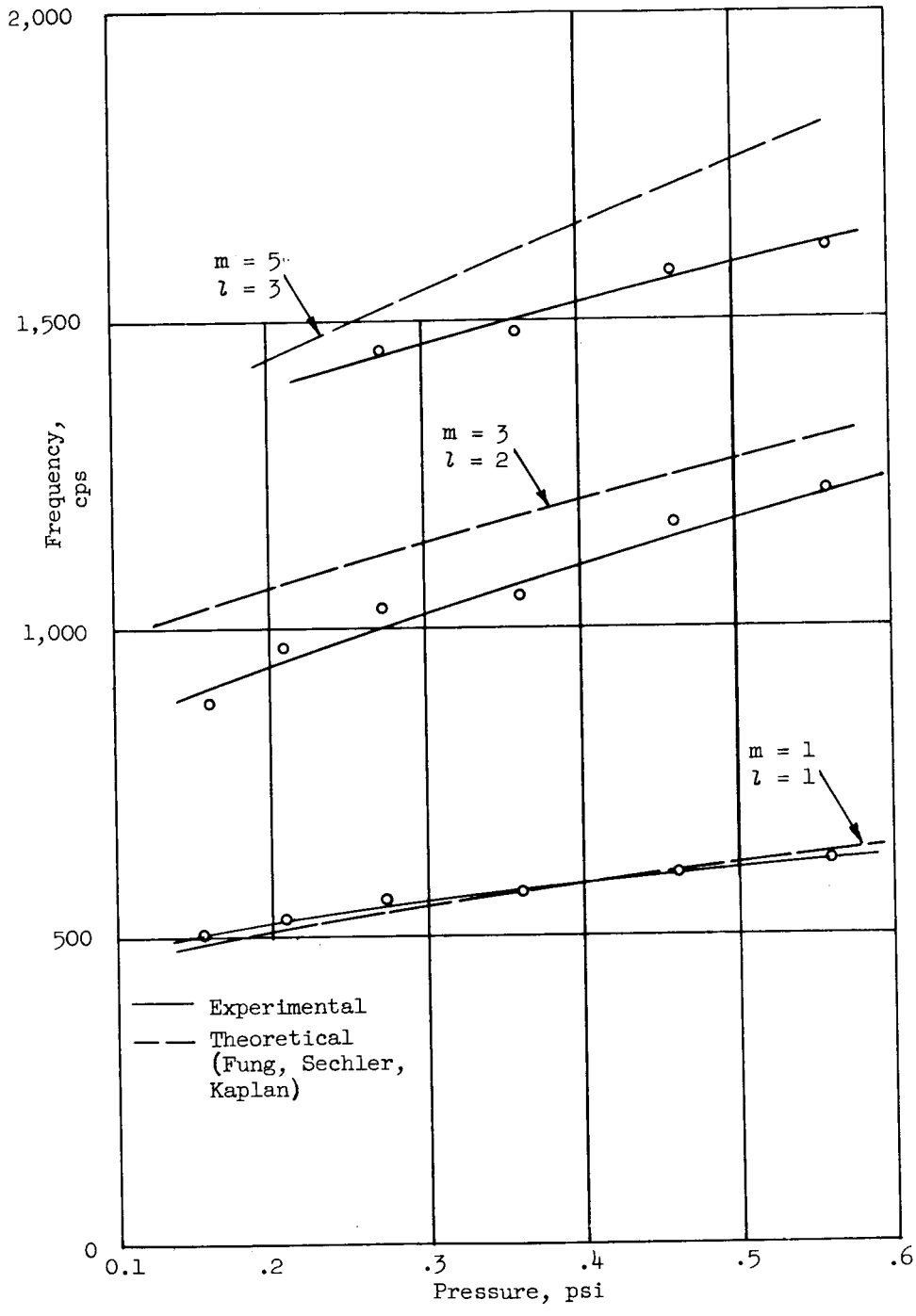


(b) Wall thickness, 0.001 inch.

Figure 17.- Continued.

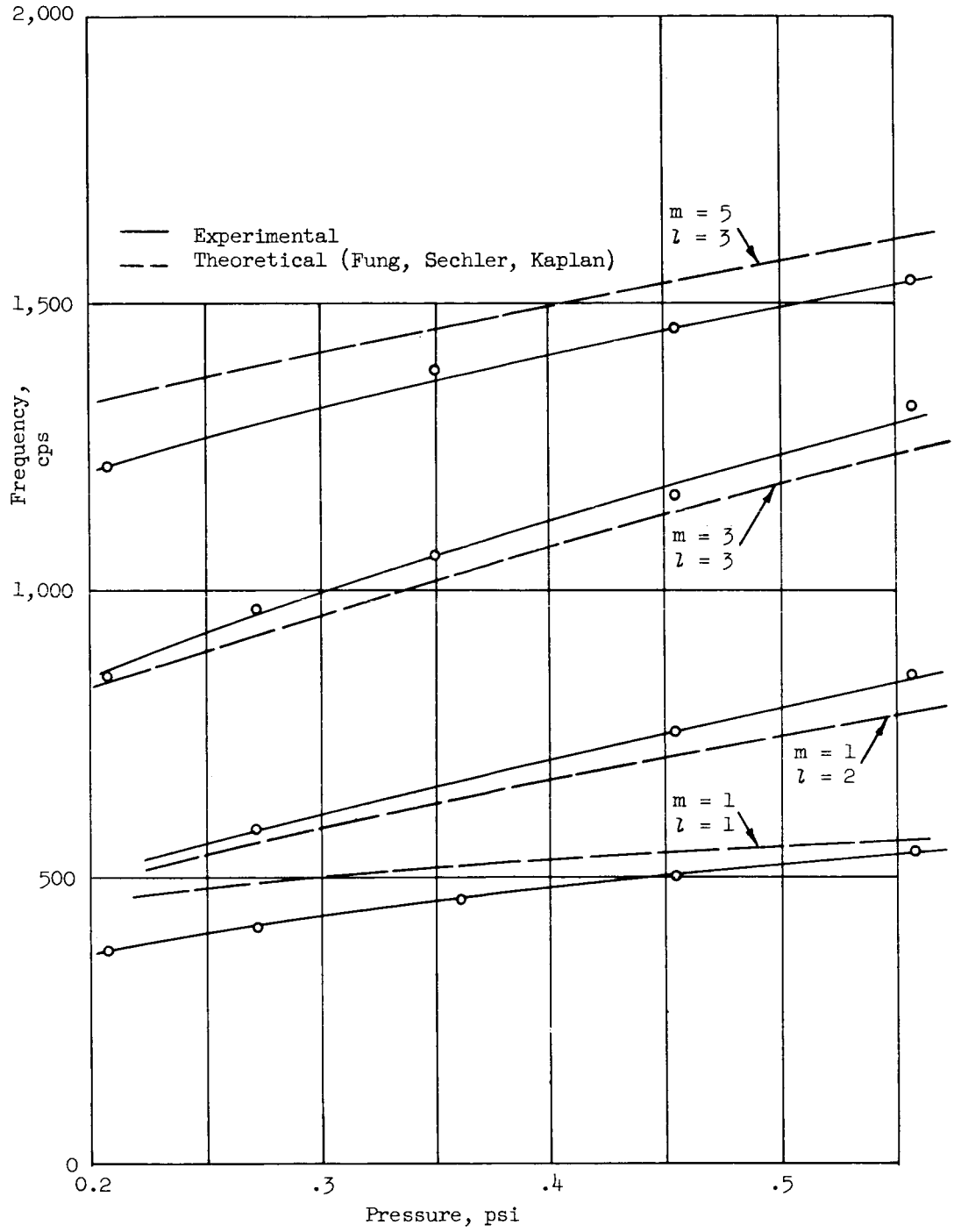


(c) Wall thickness, 0.0015 inch.

Figure 17.- Continued.

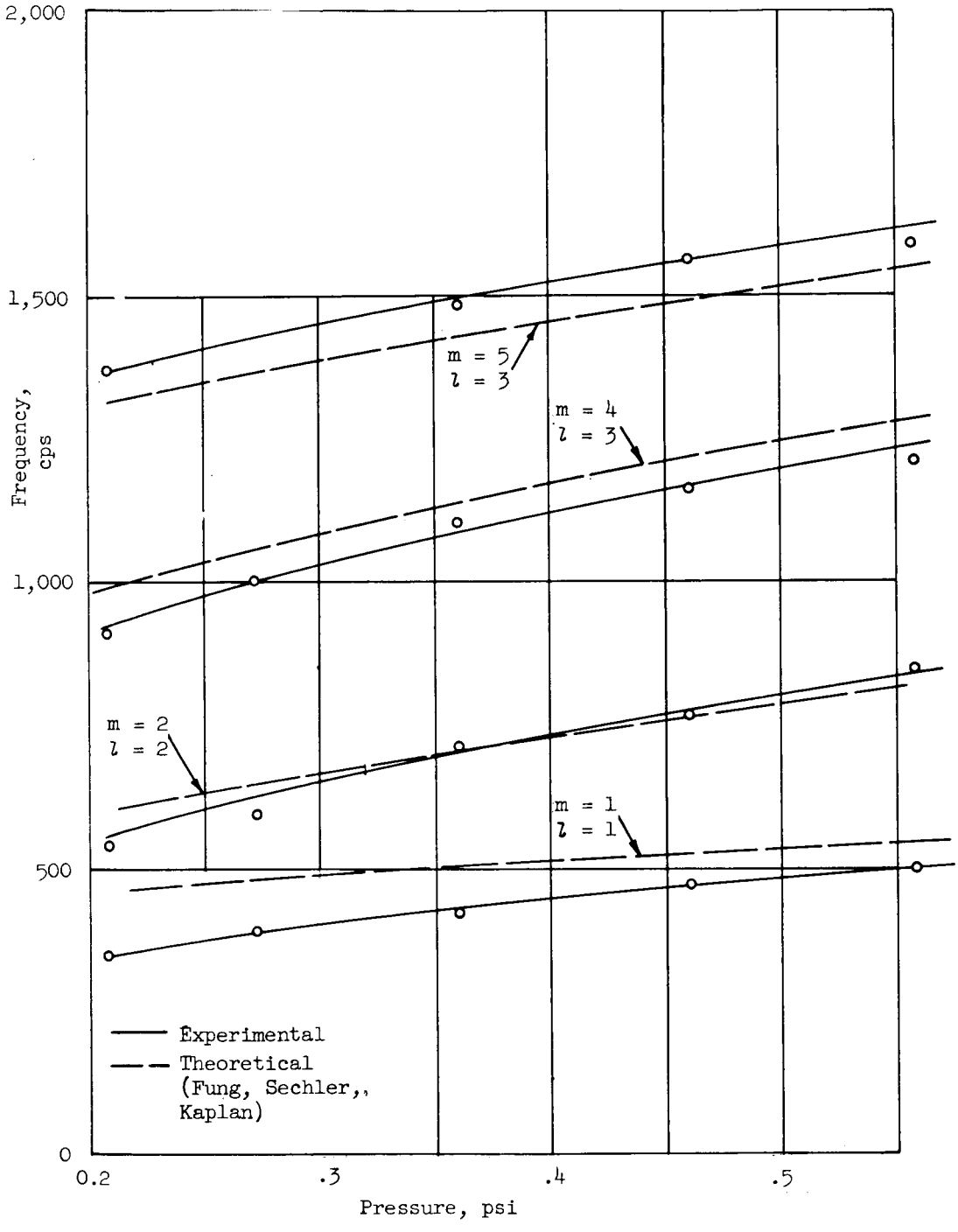


(d) Wall thickness, 0.0021 inch.

Figure 17.- Concluded.



W-128